FLAMELET GENERATED MANIFOLD

Project Report - Literature Review
Applied Combustion (ME 284)

BY

Nandola Yash Anil (Sr No: 16692)

Prof. R. V. Ravikrishna

Department of Mechanical Engineering
Indian Institute of Science
Bangalore - 560023
28 June 2020

1 Introduction and Motivation

The keywords in combustion research are efficient and clean. Efficient because our resources of fossil fuels are limited, so we have to use them wisely. Even though the use of renewable energy resources like solar and wind energy is increasing, fossil fuels will remain to be the main source of energy in the nearby decades to come. Clean is the another keyword because combustion of fossil fuels generate compounds like NO_x, carbon dioxide (CO_2), carbon monoxide (CO), which are toxic and are responsible for the greenhouse effect. So, we have to minimise their generation by improving the efficiency of the combustion appliances.

Until 1960, Combustion Research was majorly of the empirical nature and analytical work was considered for extremely simplified models only. With the advent of fast computers, and the growing of chemical kinetics during the decades, a detailed mathematical description of chemically reacting flows became available. Even then, it is still not possible to employ models that use detailed chemistry for simulation of combustion in practical furnaces. Most of the practical problems associated with combustion are of turbulent nature [20]. There are two reasons for this. First is that turbulence increases the mixing process and hence enhances combustion. Second is that, combustion releases heat and thereby generates flow instability by buoyancy and gas expansion, which then enhances transition to turbulence. It is very much difficult to solve the complete Navier-Stokes equation numerically and almost impossible to solve it analytically for the fluid flow problems.The models of turbulent flows are tremendously complicated due to large range of time and length scales involved. The modeling of laminar flames is easier, because the flow is relatively simple. The use of complex reaction mechanisms is impossible (apart from very simple cases), because for each species a PDE has to be solved, and a typical reaction mechanism for hydrocarbon combustion considers more than 100 species. Also, the chemical kinetics cause the system of differential equations to be very stiff, which makes the use of expensive implicit solvers inevitable. Thus, research is conducted on developing reduction models, which create reduced reaction models based on the complex reaction mechanism. Reduced reaction models aim to reduce the computational effort considerably without losing too much accuracy.

To model detailed dynamics and structure of chemically reacting flows, two set of techniques are used since past two decades. First one is Chemical Reduction methods used in Intrinsic Low Dimension Manifold (ILDM)[25], Computational Singular Perturbation (CSP) [23] which are based on the principle that combustion process can be modelled easily without much loss of accuracy using a few steps which are slow i.e. large time scales while considering the steps for which times scales are small to be present in partial equilibrium. This reduces stiffness of the system of PDEs to be solved and hence the complexity involved with fluid flow problem can be increased. Mathematically, this means that all variables can be stored in a lookup table as a function of few controlling variables and the equations related to these control variables only need to be solved during the run time, resulting in large savings in computation time.

Second set of techniques makes use of Laminar flamelet models [20, 18, 19] which are based on the idea that flame structures are much thinner than most scales of distortion in the flow

also implying that time scales related to chemical reactions is very fast compared to all other time scales. Hence, the internal structure of flame is almost frozen while it moves around in the flow field. Dynamics of the flame front is predicted using kinematic equation for the flame-front propagation, mixture fracture equation for the mixing and a computational fluid dynamics solver for the flow.

FGM model is a bridge between the Flamelet Model and ILDM method. [6, 14] The basic assumption of FGM and laminar flamelet approach are the same where a three dimensional complex flame can be considered as an ensemble of one-dimensional flamelets. But the implementation is more in common with the ILDM approach where a look-up table is prepared by performing flamelet simulations a-priori and the chemical states during the flamelet simulations are stored within the manifold. The manifold is subsequently parameterised by controlling variables, which are often linear combinations of mass-fractions of the species. One of the key aspects of manifold approach is to parameterise the manifold in a unique way and with as few controlling variables as possible.

The motivation behind studying FGM method is that it will help develop understanding of both set of techniques mentioned in the previous set of paragraphs used for carrying out simulations of Turbulent Combustion. Understanding of Flamelet Techniques will be developed by understanding how flamelet equations are derived in FGM by carrying out coordinate transformation to orthogonal curvilinear coordinates which is attached to the flame front. By applying this transformation, we obtain set of quasi 1-D flamelets and the ensemble of these flamelets can be used to model the complete flame in 3-dimensional space.

By understanding how to construct manifold from solution of these flamelet equations, we will develop an understanding of Chemical Reduction Techniques where a lookup table is prepared to store thermo-chemical properties of the system, as done in ILDM method. Here, flamelet simulations are performed using detailed chemical reactions and solution is stored as a function of control variables thus generating a low-dimension manifold. A better understanding of what a manifold is and how the lookup table is generated will be obtained when we reach the section Flamelet to Manifold. This lookup table can be then integrated with the CFD flow solver to finally solve the complex Combustion Problem.

The implementation of Flamelet Generated Model consists of three important steps:
1. Computing representative flamelets
2. Building a look-up table
3. Coupling the table with a flow solver

Figure 1 shows how FGM method can be used to solve problems related to Combustion. Solid arrows indicate actual Combustion Simulation process and dashed arrows indicate that FGM lookup table is generated a-priori and required data are extracted from this lookup table. It is seen how transport equations are to be solved only for the control variables, hence reducing the cost of computation of the process.

Further ahead in this study, first of all flamelet equations are derived by performing coordinate transformation to convert a 3-dimensional flame into quasi-one-dimensional flamelet. Then, it is discussed briefly how manifolds are generated by solving these flamelet equations

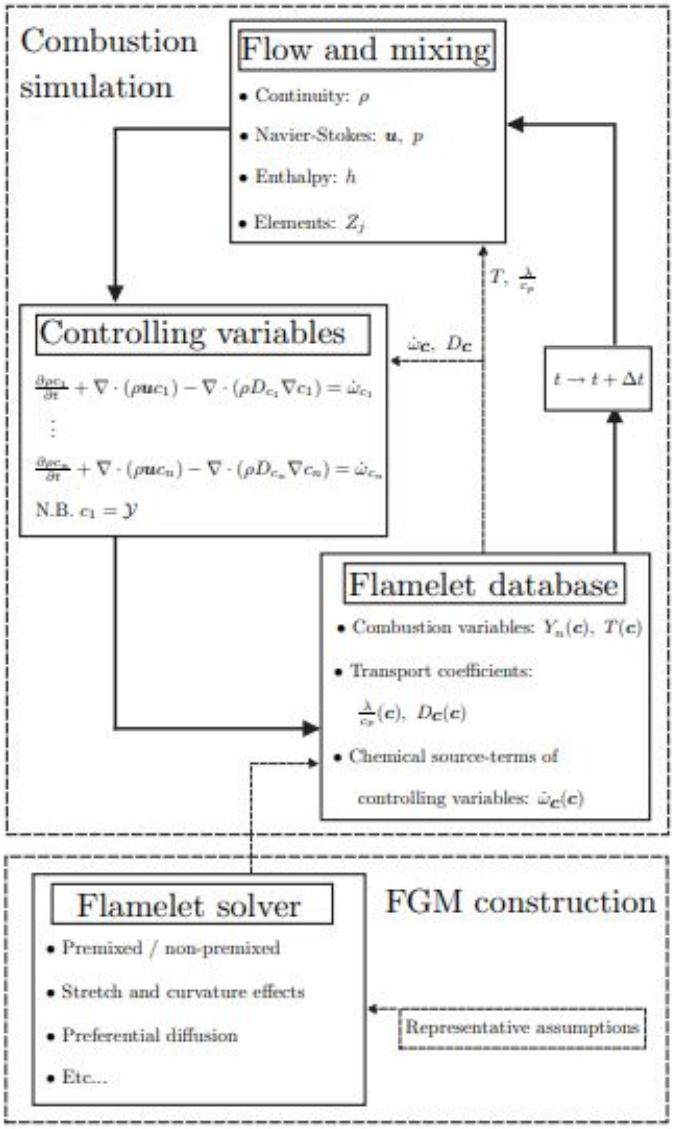

Figure 1: Flow Diagram of solving procedure using a pre-computed Flamelet Generated Manifold (Source: Delhaye S., Incorporating unsteady flow-field effects in flamelet-generated manifolds, [Ph. D. thesis], Eindhoven University of Technology; 2009)

which are parameterised in terms of controlling variables and stored in a lookup table. Then it is further discussed how look-up table data can be integrated with a CFD-solver to obtain the solution for the entire-flow field. Finally, few cases where FGM model is applied in various combustion problems is discussed along with the brief results and conclusions of the application of method.

2 Flamelet Equations

Unified Flamelet Model, used in FGM is presented first[6]. It is capable of modeling premixed, non-premixed and partially-premixed flames. The combustion problem is decomposed into three distinct subproblems:
1. fluid motion and mixing of enthalpy and elements
2. the flame front dynamics
3. the internal flame structure embedded within this flame front.

We construct a low-dimensional manifold by deriving quasi-one dimensional flamelet equations by performing coordinate transformation on conservation laws which are originally present in Tensorial Form. The low dimensional manifold is parameterised by reduced number of controlling variables. Such a manifold is generated a-priori and stored in the form of a lookup table. Then during complex combustion simulations, thermo-physical data is retrieved from the lookup table as a function of controlling variables, where transport equations are solved for reduced number of controlling variables instead of complete set of stiff PDEs along with the flow equations (Continuity and Momentum Equation). This brings down the computational effort by great levels. Each of the three sub-problems which describe the flame front dynamics along with internal structure of the flame using representative flamelets to obtain set of flamelet equations are described in the following sections of this chapter. In this work, only description of steps involved with FGM are described. For detailed mathematical description of derivation of flamelet equations, please refer [14, 6, 22].

2.1 Fluid Motion and Mixing of Enthalpy and Elements

The evolution of chemically reacting flows is governed by a set of transport equations describing the conservation of mass, momentum energy and chemical components. We will formulate these conservation laws as well as these constitutive relations. Models are presented for the diffusion velocity of species, for the stress tensor and for the heat flux vector. For more detailed derivations of Conservation Equations, please refer [4] and [7]

For a mixture of N_s species, we can write density of the mixture to be equal to $\sum_{i=1}^{N_s} \rho_i = \rho$. Now we can define bulk mass weighted velocity $\boldsymbol{v}$ as the resultant of the individual velocities $\boldsymbol{v_i}$ of the various species. Thus, by definition:

$$\sum \rho_i \boldsymbol{v_i} = \rho \boldsymbol{v} \tag{1}$$

The difference between $\boldsymbol{v_i}$ and $\boldsymbol{v}$ is the molecular diffusion velocity given as $\boldsymbol{V_i} = \boldsymbol{v_i} - \boldsymbol{v}$. Using the two relationships just above, we can write $\sum_{i=1}^{N_s} \rho_i \boldsymbol{V_i} = \sum_{i=1}^{N_s} \rho_i \boldsymbol{v_i} - \sum_{i=1}^{N_s} \rho \boldsymbol{v}$. In terms of mass fractions for individual species $Y_i = \rho_i/\rho$, we can write $\boldsymbol{v} = \sum_{i=1}^{N_s} Y_i \boldsymbol{v_i}$ and $\sum_{i=1}^{N_s} Y_i \boldsymbol{V_i} = 0$. Overall conservation of mass is expressed by the continuity equation:

$$\frac{\partial \rho}{\partial t} + \nabla \cdot (\rho \boldsymbol{v}) = 0 \tag{2}$$

where ρ is the mass density and $\boldsymbol{v} = (u, v, w)^T$ is the velocity of the gas mixture. Mass conservation for individual species present in the mixture can be written as:

$$\frac{\partial \rho_i}{\partial t} + \nabla \cdot [\rho_i(\boldsymbol{v} + \boldsymbol{V_i})] = \dot{\omega}_i, \quad i \in [1, N_s] \tag{3}$$

where $\dot{\omega}_i$ is the mass reaction rate or the chemical source term which gives the rate of mass of species i generated per unit volume. Since chemical reactions are mass conserving, $\sum_{i=1}^{N_s} \dot{\omega}_i = 0$. Now use the relationship $\rho_i = Y_i \rho$ and simplifying the equations

$$\frac{\partial \rho Y_i}{\partial t} + \nabla \cdot (\rho \boldsymbol{v} Y_i) = -\nabla \cdot (\rho \boldsymbol{V_i} Y_i) + \dot{\omega}_i \tag{4}$$

Source term

$$\dot{\omega}_i = W_i \sum_{l=1}^{K} (\nu''_{i,l} - \nu'_{i,l}) B_l T^{\alpha l} exp(-E_{a,l}/R_u T) \prod_{j=1}^{N_s} c_j^{\nu'_{j,l}} \tag{5}$$

$$= W_i \sum_{1=1}^{K} (\nu''_{i,l} - \nu'_{i,l}) k_l^f \prod_{j=1}^{N_s} (\frac{\rho Y_i}{W_i})^{\nu'_{j,l}} - k_l^b \prod_{j=1}^{N_s} (\frac{\rho Y_i}{W_i})^{\nu''_{j,l}} \qquad i \in [1, N_s] \tag{6}$$

where k_l is the reaction rate constant for reaction l. $\nu''_{j,l}, \nu'_{j,l}$ are stoichiometric coefficients of the reaction $\sum_{i=1}^{N_s} \nu'_i M_i \rightarrow \sum_{i=1}^{N_s} \nu''_i M_i$ Multi-component Diffusion Equation provides relationship between the concentration gradient X_i and Diffusion Velocity $\boldsymbol{V_i}$. The equation is as follows:

$$\nabla X_i = \sum_{j=1}^{N_s} (\frac{X_i X_j}{D_{i,j}})(\boldsymbol{V_j} - \boldsymbol{V_i}) + (Y_i - X_i)(\frac{\nabla p}{p}) + (\frac{p}{\rho}) \sum_{j=1}^{N_s} Y_i Y_j (\boldsymbol{f_i} - \boldsymbol{f_j}) + \sum_{j=1}^{N_s} [(\frac{X_i X_j}{\rho D_{i,j}})(\frac{D_{T,j}}{Y_j} * \frac{D_{T,i}}{Y_i})](\frac{\nabla T}{T})$$
$$i \in [1, N_s] \tag{7}$$

For the terms present in RHS, the first term represents Fickian Diffusion in the presence of Concentration Gradient. The second term represents diffusion in the presence of a pressure gradient, the third one in the presence of body force $\boldsymbol{f_i}$ and the final term represents Second-Order Soret Diffusion in the presence of temperature gradient. We obtain Stefan-Maxwell Relationship in the absence of pressure-gradient, body force and second order diffusion effect (Soret Effect).

$$\nabla ln X_i = \sum_{i=1}^{N_s} (\frac{X_j}{D_{i,j}})(\boldsymbol{V_j} - \boldsymbol{V_i}) \qquad i \in [1, N_s] \tag{8}$$

$D_{i,j}$ is the binary diffusion mass diffusion coefficient of species i into species j. We will simplify 8 by using model based on Fick's Law of mass diffusion, which is commonly used to model diffusion velocities [13]. The diffusion velocities are defined as:

$$\boldsymbol{V_i} = -\frac{D_{i,m}}{Y_i} \nabla Y_i \qquad i \in [1, N_s] \tag{9}$$

where $D_{i,m}$ is the diffusion coefficient of species i into mixture m, which can be related to overall diffusion coefficient D as:

$$Di, m = \frac{D}{Le_i} \tag{10}$$

where overall diffusion coefficient is given as:

$$D = \frac{\lambda}{\rho c_p} \tag{11}$$

Lewis number, which is the ratio of thermal conduction and species mass diffusion is defined as:

$$Le_i = \frac{\lambda}{\rho D_{i,m} c_p} \qquad i \in [1, N_s] \tag{12}$$

Ratio between thermal conductivity and specific heat can be calculated using a simplified relation which is a function of temperature only. From the definition of Lewis number, 9 becomes:

$$\boldsymbol{V_i} = -\frac{D}{Le_i Y_i} \nabla Y_i \qquad i \in [1, N_s] \tag{13}$$

where it is assumed that Lewis number is constant throughout the flame. Thus using 13, 4 becomes:

$$\frac{\partial \rho Y_i}{\partial t} + \nabla \cdot (\rho \boldsymbol{v} Y_i) - \frac{1}{Le_i} \nabla \cdot (\rho D \nabla Y_i) = \dot{\omega}_i \quad i \in [1, N_s] \tag{14}$$

14is the Species Conservation equation. Conservation of momentum is given by Navier-Stokes equation:

$$\frac{\partial \rho \boldsymbol{v}}{\partial t} + \nabla \cdot (\rho \boldsymbol{v} \otimes \boldsymbol{v}) = -\nabla \cdot \boldsymbol{P} + \rho \sum_{i=1}^{N_s} Y_i \boldsymbol{f_i} \tag{15}$$

where, $\boldsymbol{P}$ is the stress tensor and $\boldsymbol{f_i}$ is the volumetric force (body force), represents all the external forces per unit mass acting on the individual species i. No other body forces except gravity are considered for this case. Constitutive Relationship for Pressure Tensor $\boldsymbol{P}$ is as follows:

$$\boldsymbol{P} = p\boldsymbol{U} - \boldsymbol{\tau} \tag{16}$$

$$\boldsymbol{\tau} = \mu[(\nabla \boldsymbol{v}) + (\nabla \boldsymbol{v}^T) - 2/3(\nabla \cdot \boldsymbol{v})\boldsymbol{U}] \tag{17}$$

Here, $\boldsymbol{U}$ is the Unit Matrix, $\boldsymbol{\tau}$ is the viscous stress tensor. We will neglect all the types of body forces for this formulation. Thus the required momentum equation is:

$$\frac{\partial \rho \boldsymbol{v}}{\partial t} + \nabla \cdot (\rho \boldsymbol{v} \otimes \boldsymbol{v}) = -\nabla p + \nabla \cdot \boldsymbol{\tau} \tag{18}$$

Now we will write energy conservation:

$$\frac{\partial(\rho e)}{\partial t} + \nabla \cdot (\rho \boldsymbol{v} e) = -\nabla \cdot \boldsymbol{q} - \boldsymbol{P} : (\nabla \boldsymbol{v}) + \rho \sum_{i=1}^{N_s} Y_i \boldsymbol{f_i} \cdot \boldsymbol{V_i} \tag{19}$$

where $\boldsymbol{q}$ denotes heat flux. Second term of the RHS is enthalpy production due to viscous effects and the third term is due to body forces. It is assumed that there are no volumetric heat sources. Here we can write: $h = \sum_{i=1}^{N_s} Y_i h_i$ with $h_i = h_i^0 + \int_{T_{ref}}^{T} c_p(\eta) d\eta$. This is the first equation required to close the problem. Second equation to close the problem is the ideal gas equation of state(In most combustion problems, the gas mixture and its components are considered to behave as ideal gases).
$\rho = \frac{pM_{mix}}{R_u T}$, where R_u is the Universal Gas Constant and M_{mix} is the Molecular weight of mixture of ideal gases which is equal to: $M_{mix} = (\sum_{i=1}^{N_s} Y_i/M_i)^{-1}$, where M_i is the molecular weight of species i. The constitutive relationship for Heat Flux Vector $\boldsymbol{q}$ is as follows:

$$\boldsymbol{q} = -\lambda \nabla T + \rho \sum_{i=1}^{N} h_i Y_i \boldsymbol{V_i} + R_u T \sum_{i=1}^{N} \sum_{j=1}^{N} (\frac{X_j D_{T,i}}{W_i D_{i,j}})(\boldsymbol{V_i} - \boldsymbol{V_j}) + \boldsymbol{q_R} \tag{20}$$

The first term represents heat transfer via Conduction in the presence of Temperature Gradient. Second term is energy transfer in the form of heat due to different heat contents of various species. This term goes to zero when the specific heats of different species are the same. The third term represents second-order diffusion, the Dufour Effect, accounting for the heat transfer in the presence of mass diffusion, especially due to the concentration gradient. This term exists even if the specific heats of various species are the same in our given mixture unlike the second term. Fourth and the final term is the heat transfer due to radiation. This term depends on temperature of the gas and the molecular structure, because the efficiency of molecular radiation absorption and emission is sensitive to wavelength of the radiation. This mode of heat transfer is important for the flames with heavy soot loading.

We neglect Dufour effect and energy transfer due to radiation. Also in low subsonic combustion, viscous heating is much weaker than heat involved with other modes of heat transfer and chemical heat release. Also the changes in enthalpy caused due to pressure change are neglected (Dp/Dt = 0). We substitute internal energy as e = h - p/ρ. Thus we can write:

$$\boldsymbol{P} : (\nabla \boldsymbol{v}) = p\boldsymbol{U} : (\nabla \boldsymbol{v}) = p \nabla \cdot \boldsymbol{v} \tag{21}$$

$$\frac{\partial}{\partial t}(\rho h) + \nabla \cdot (\rho \boldsymbol{v} h) = -\nabla \cdot \boldsymbol{q} \tag{22}$$

$$\boldsymbol{q} = -\lambda \nabla T + \sum_{i=1}^{N_s} \rho \boldsymbol{V_i} Y_i h_i = -\lambda \nabla T - \sum_{i=1}^{N_s} \frac{\rho D}{Le_i} \nabla (Y_i h_i) \tag{23}$$

$$h = \sum_{i=1}^{N_s} Y_i h_i \tag{24}$$

$$\nabla h = \sum_{i=1}^{N_s} h_i \nabla Y_i + \sum_{i=1}^{N_s} Y_i \nabla h_i = \sum_{i=1}^{N_s} h_i \nabla Y_i + c_p \nabla T \tag{25}$$

$$\Rightarrow \frac{\partial(\rho h)}{\partial t} + \nabla \cdot (\rho \boldsymbol{v} h) - \nabla \cdot (\rho D h) = \sum_{i=1}^{N_s} (\frac{1}{Le_i} - 1) \nabla \cdot (\rho D h_i \nabla Y_i) \quad \text{(From 8, 9, 19, 20, 22)} \tag{26}$$

We will summarise conservation equations that we have obtained till now. We have N_s + 5 conservation equations (1 Continuity, N_s species mass conservation, 3 Momentum conservation, 1 Energy Conservation), 2 state equations (1 enthalpy at a temperature and second Ideal Gas equation of state). Also we have N_s + 7 variables ($\rho, \boldsymbol{v}$, p, h, T, and N_s species mass fractions Y_i).

Also element mass fractions are taken into consideration, which are defined as:

$$Z_j = \sum_{i=1}^{N_s} w_{ji} Y_i \qquad j \in [1, N_e] \tag{27}$$

where w_{ji} denotes the mass fraction of element j in species i. Taking appropriate linear combination of 14, we can obtain conservation equation for element mass fraction as:

$$\frac{\partial(\rho Z_j)}{\partial t} + \nabla \cdot (\rho \boldsymbol{v} Z_j) - \nabla \cdot (\rho D Z_j) = \sum_{i=1}^{N_s} (\frac{1}{Le_i} - 1) \nabla \cdot (\frac{\lambda}{c_p} w_{ji} \nabla Y_i) \tag{28}$$

Element conservation equation is not independent of the species conservation equation. Energy conservation and element conservation equations have quite some resemblance, both do not contain any source terms, and hence influenced in the flame only by convection and diffusion. When Lewis number equals to 1, all element mass fractions and enthalpy equations behave the same.

Thus, final set of flow, energy and species reaction that we have along with us are as follows:

$$\frac{\partial \rho}{\partial t} + \nabla \cdot (\rho \boldsymbol{v}) = 0 \tag{29}$$

$$\frac{\partial(\rho \boldsymbol{v})}{\partial t} + \nabla \cdot (\rho \boldsymbol{v} \otimes \boldsymbol{v}) = -\nabla p + \nabla \cdot \boldsymbol{\tau} \tag{30}$$

$$\frac{\partial(\rho h)}{\partial t} + \nabla \cdot (\rho \boldsymbol{v} h) - \nabla \cdot (\frac{\lambda}{C_p} \nabla h) = \nabla \cdot (\frac{\lambda}{C_p} \sum_{i=1}^{N_s} (\frac{1}{Le_i} - 1) h_i \nabla Y_i) \tag{31}$$

$$\frac{\partial(\rho Y_i)}{\partial t} + \nabla \cdot (\rho \boldsymbol{v} Y_i) = -\nabla \cdot (\rho \boldsymbol{V_i} Y_i) + \dot{\omega}_i \qquad i = 1, 2, 3, ..., N_s - 1 \tag{32}$$

$$\frac{\partial(\rho Z_j)}{\partial t} + \nabla \cdot (\rho \boldsymbol{v} Z_j) - \nabla \cdot (\frac{\lambda}{C_p} \nabla Z_j) = \nabla \cdot (\frac{\lambda}{C_p} \sum_{i=1}^{N_s} (\frac{1}{Le_i} - 1) w_{j,i} \nabla Y_i) \qquad j = 1, 2, ..., N_e - 1 \tag{33}$$

2.2 Flame Front Dynamics [6]

Following the traditional Flamelet Methods, a flame is described as the region in the spatial domain, where $y_1 \leq y \leq y_2$ for a certain scalar variable y (which is known as controlling variable in case of FGM method, which is usually mass fraction of product species like CO_2 for premixed flames and mixture fraction Z for non-premixed flames). The subscripts 1 and 2 indicate boundaries of the flame. In premixed flames, the flame separates unburnt mixture from the burnt mixture and in non-premixed flames, fuel side is separated by the flame from oxidiser side. The controlling variable is so chosen that $\nabla y \neq 0$ holds in the entire domain. Flame surfaces are now defined as iso-surfaces of y where $y(\boldsymbol{x}, t) = y_0$ for some constant y_0. It will be shown in this section that dynamics of flame front (undergoes translation, stretching, compression, wrinkling in the space) which is described as the solution of kinematic equation of the progress variable is equivalent to solving transport equation for the progress variable within the domain. The kinematic equation is given as follows:

$$\frac{dy}{dt} = \frac{\partial y}{\partial t} + \boldsymbol{v_f} \cdot \nabla y = 0 \tag{34}$$

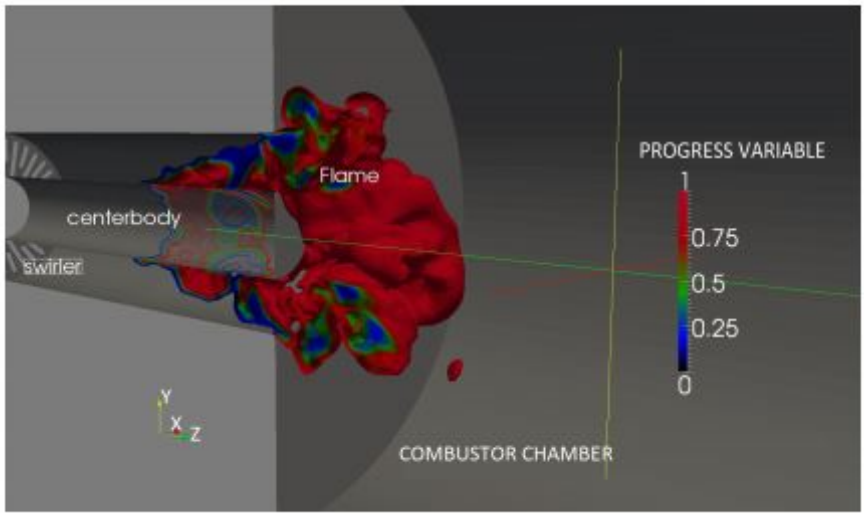

Figure 2: 3 D Instantaneous Flame front shown as iso-surface of the mean progress variable.(Source: Cardoso de Souza, T., Bastiaans, R. J. M., Geurts, B. J., and De Goey, L. P. H.,LES and RANS of Premixed Combustion in a Gas-Turbine Like Combustor Using the Flamelet Generated Manifold Approach, Proceedings of the ASME 2011 Turbo Expo: Turbine Technical Conference and Exposition.)

which means that the point on an iso-surface of y stays on that surface for all times t. The transient behaviour of progress variable y, and hence the dynamics of the flame front can be obtained by obtaining solution of this kinematic equation 34. But to obtain the solution, we need to determine flame speed $\boldsymbol{v_f}$.

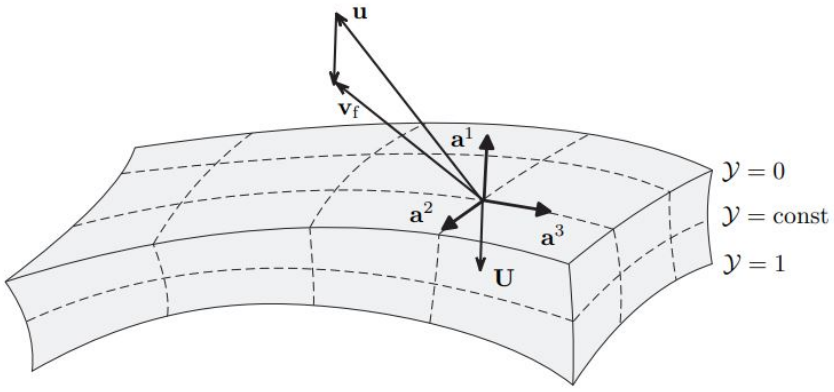

Figure 3: Schematic Representation of a flame front. Several flame surface, which are iso-surfaces of controlling variable y. Three velocity vectors are shown $\boldsymbol{u}$: Fluid Velocity $\boldsymbol{v}$, $\boldsymbol{U}$: Displacement velocity of iso-surfaces of y, $\boldsymbol{v_f}$: Flame Speed. (Source: Delhaye S., Incorporating unsteady flow-field effects in flamelet-generated manifolds, [Ph. D. thesis], Eindhoven University of Technology; 2009)

We introduce flame adapted orthogonal co-ordinate system for which the basis vectors are chosen such that $\boldsymbol{a^1}$ is normal to the iso-surfaces of y and $\boldsymbol{a^2}$ *and* $\boldsymbol{a^3}$ are orthogonal to each other and also to $\boldsymbol{a^1}$. We also have three velocities represented in figure 3 which are fluid velocity $\boldsymbol{v}$(given in figure 3 as $\boldsymbol{u}$), displacement velocity of iso-surfaces $\boldsymbol{U}$ and velocity of the flame-front $\boldsymbol{v_f}$. These three are related to each other as follows:

$$\boldsymbol{v_f} = \boldsymbol{U} + \boldsymbol{v} \tag{35}$$

For the evolution of iso-surfaces of y, normal velocity component is relevant, hence we will decompose the flame-velocity into its normal and tangential components as follows:

$$\boldsymbol{v_f} = \boldsymbol{v_f^n} + \boldsymbol{v_f^t} \tag{36}$$

where $\boldsymbol{v_f^n}$ describes actual movement of the flame front. Now the iso-surfaces only have velocity in the direction normal to the iso-surfaces, $\boldsymbol{U} = U\boldsymbol{n}$, where the normal $\boldsymbol{n}$ is defined as:

$$\boldsymbol{n} = -\frac{\boldsymbol{a^1}}{|\boldsymbol{a^1}|} = -\frac{\nabla y}{|\nabla y|} \tag{37}$$

This means that, if $y = Y_{CO_2}/Y_{H_2O}$, then normal points towards the unburnt side of the mixture for a premixed flame. For a non-premixed flame, when $y = \mathrm{Z}$ is chosen, normal points towards the oxidiser side. Thus, we can write the components of the flame velocity as follows:

$$\boldsymbol{v_f^n} = U\boldsymbol{n} + \boldsymbol{v^n} \tag{38}$$

$$\boldsymbol{v_f^t} = \boldsymbol{v^t} \tag{39}$$

where $\boldsymbol{v^n}$ is the normal component of the fluid velocity and $\boldsymbol{v^t}$ is the tangential one. The evaluation of tangential velocity of the flame front is straight forward, it is merely the tangential component of the local fluid velocity. To evaluate the normal component of the flame speed, we first need to determine $\boldsymbol{U}$. We can take a different path to avoid this issue. We can use the conservation equation of primary control variable y in order to determine velocity of the flame front $\boldsymbol{v_f}$. Conservation equation for y can be written as:

$$\frac{\partial(\rho y)}{\partial t} + \nabla \cdot (\rho \boldsymbol{v} y) - \nabla \cdot (\rho D_y \nabla y) = \dot{\omega}_y \tag{40}$$

This equation describes local change in y due to imbalance in diffusion, convection and chemical reactions. When equation 40 is combined with continuity equation, and the equation is subsequently divided by ρ, we obtain following equation:

$$\frac{\partial y}{\partial t} + \boldsymbol{v} \cdot \nabla y = \frac{\dot{\omega}_y + \nabla \cdot (\rho D_y \nabla y)}{\rho} \tag{41}$$

Now we subtract 41 from 34, we obtain

$$(\boldsymbol{v_f} - \boldsymbol{v}) \cdot \nabla y = \frac{\dot{\omega}_y + \nabla \cdot (\rho D_y \nabla y)}{\rho} \tag{42}$$

Divide the given equation by $|\nabla y|$, we obtain speed of the iso-surfaces of y given as

$$U = \frac{\dot{\omega}_y + \nabla \cdot (\rho D_y \nabla y)}{\rho |\nabla y|} \tag{43}$$

Thus solving 34 in conjunction with 43 is equivalent to solving conservation equation for the primary control variable y, 40. In FGM, we solve the conservation equation of y to model flame front dynamics.

2.3 Internal Flame Dynamics [6]

Now as we have located the flame in three dimensional space at a particular instant of time as collection of flamelets (which are themselves iso-surfaces of a scalar) as discussed in the previous section, we will now look at the internal structure of the flame. Within the flamelet regime, multi-dimensional flame can be considered as a collection od 1-D flamelets. We bring in the flame adopted coordinate system to convert 3-D flame model equations into 1-D model equations. Orthogonal curvilinear coordinate system is introduced for that purpose by van Oijen [14, 6]. By proper introduction of this coordinate system, the resulting model is decomposed in contributions normal to the flame surface and the contribution which is taking place within the flame surface themselves. The curvilinear coordinate system which is introduced, is such that $y(\boldsymbol{x}, t) = y(\xi^1)$, which implies that iso-surfaces of ξ^1 are also iso-surfaces of y and the velocity at which this coordinate system moves is equal to the velocity of the flame itself i.e. $(\boldsymbol{v_f} - \dot{\boldsymbol{x}}) \cdot \boldsymbol{a^1} = 0$, where $\dot{\boldsymbol{x}}$ is the velocity of the coordinate system.

Mass based stretch rate was introduced by De Goey et al. [17] which is related to rate of change of mass M(t) contained in an infinitesimal volume V(t) in the flame as $K = \frac{1}{M}\frac{dM}{dt}$. Applying Reynolds Transport Theorem to the definition of mass within an infinitesimal volume $M(t) = \int_{V(t)} \rho dV$, we obtain:

$$\rho K = \frac{\partial \rho}{\partial t} + \nabla \cdot (\rho \boldsymbol{v_f}) \tag{44}$$

We define ∂s as arc length in direction normal to the plane for curvilinear orthogonal coordinate and σ as the flame surface area across which the transport takes place. We also define local mass burning rate m = ρU, where U is defined in flame front dynamics section. Subtract 2 from 44and using definition of flame velocity, we can obtain:

$$\frac{\partial m}{\partial s} = -\rho K_m + m\kappa \tag{45}$$

where $\kappa = \nabla \cdot \boldsymbol{n} = -\frac{1}{\sigma}\frac{\partial \sigma}{\partial s}$ is the local curvature of the flame surface. 45 represents quasi 1-D form of continuity equation in transformed coordinate frame of reference. When similar coordinate transformation is performed for energy equation, conservation equations of species mass fractions and scalar (principle controlling variable), we obtain following set of equations:

$$\frac{\partial F_y}{\partial s} - \dot{\omega_y} = -\rho K y + F_y \kappa \tag{46}$$

$$\rho\frac{\partial Y_i}{\partial \tau} + \frac{\partial F_i}{\partial s} - \dot{\omega_i} = -\rho K Y_i + F_i + Q_i \qquad i \in [1, N_s] \tag{47}$$

$$\rho\frac{\partial h}{\partial \tau} + \frac{\partial F_h}{\partial s} = -\rho K h + F_h \kappa + Q_h \tag{48}$$

where $\frac{\partial(...)}{\partial \tau} = \frac{\partial(...)}{\partial t} + \dot{x} \cdot \nabla(...)$ is the temporal derivative in transformed coordinate system. F_y, F_i, F_h represent fluxes of principle controlling variable, species and enthalpy respectively, which are given as:

$$F_y = my - \rho D_y \frac{\partial y}{\partial s} \tag{49}$$

$$F_i = mY_i - \rho D_i \frac{\partial Y_n}{\partial s} \quad i \in [1, N_s] \tag{50}$$

$$F_h = mh - \frac{\lambda}{c_p}\frac{\partial h}{\partial s} - \frac{\lambda}{c_p}\sum_{i=1}^{N_s}(\frac{1}{Le_i} - 1)h_i \frac{\partial Y_i}{\partial s} \tag{51}$$

and terms on right hand side of equations 47,48 $Q_i and Q_h$ represent the diffusion of species and enthalpy along the flame surfaces which are given as:

$$Q_i = \rho(\boldsymbol{v_{fi}} - \boldsymbol{v_f}) \cdot \nabla Y_i + \nabla \cdot (\frac{\lambda}{Le_i c_p}\nabla_{||} Y_i) \tag{52}$$

$$Q_h = \rho(\boldsymbol{v_{fh}} - \boldsymbol{v_f}) \cdot \nabla h + \nabla \cdot (\frac{\lambda}{c_p}\nabla_{||} h + \frac{\lambda}{c_p}\sum_{1=1}^{Ns}(\frac{1}{Le_i} - 1)h_i \nabla_{||} Y_i) \tag{53}$$

where $\nabla_{||}$ represents gradient operator in tangential direction in transformed coordinate system and $\boldsymbol{v_{fi}}, \boldsymbol{v_{fh}}$ represents velocity of iso surfaces of Y_i and h respectively. Right hand side in equations 45, 46, 47, 48 represents deviations from one-dimensional flat flame behaviour. These four equations together form a set known as flamelet equations. Usually lookup table is generated for two archetypal types of flamelets: laminar premixed, adiabatic, stretchless freely propagating flame and counter-flow diffusion flame. Flamelet equations get simplified for these two types of flamelets which is discussed ahead in this section.

2.3.1 Laminar Premixed Flamelet

In a premixed flamelet, a stream of perfectly premixed fuel and oxidiser is converted into combustion products when it passes through the reactive layer. The system is treated as an adiabatic, freely-propagating, premixed flat flame. Combustion variables ρ, T, Y_i and gas velocity depend on the x-coordinate perpendicular to the flame surface. The flamelet is stretchless (indicating no loss of mass perpendicular to the flame coordinate system), K = 0. The flamelet equations reduce to:

$$\frac{\partial \rho u}{\partial x} = 0 \tag{54}$$

$$\frac{\partial \rho u Y_i}{\partial x} = \frac{\partial}{\partial x}(\frac{\lambda}{Le_i c_p}\frac{\partial Y_i}{\partial x}) + \dot{\omega}_i, \quad i \in [1, N_s - 1] \tag{55}$$

$$\frac{\partial \rho u h}{\partial x} = \frac{\partial}{\partial x}[\frac{\lambda}{c_p}\frac{\partial h}{\partial x} + \frac{\lambda}{c_p}\sum_{i=1}^{N_s}(\frac{1}{Le_i} - 1)h_i\frac{\partial Y_i}{\partial x}] \tag{56}$$

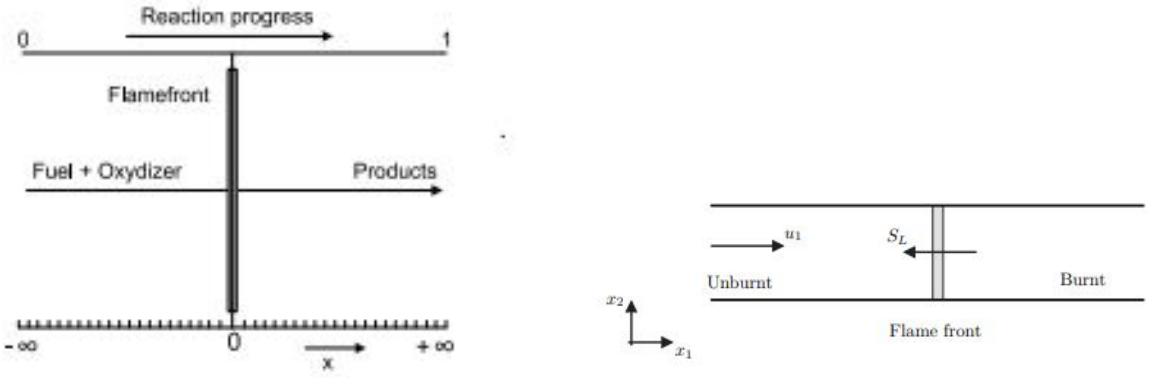

(a) (b)

Figure 4: Scematic Representation of premixed flamelets (Source: [22] (left) and [6] (right))

$\partial s = \partial x$ in this case and for steady flame m = ρU. At the un-burnt side, Dirichlet boundary conditions are applied for Y_i and h, while Neumann boundary conditions are applied at the

burnt side. Mass burning rate is the eigen value of the flamelet equations described above and for adiabatic flamelets, $u = s_d$ is commonly referred as burning velocity s_L.

$$Y_i(x \to -\infty) = Y_{i,-\infty}, \quad h(x \to -\infty) = h_{-\infty} \tag{57}$$

$$\frac{\partial Y_i}{\partial x}(x \to \infty) = 0, \quad \frac{\partial h}{\partial x}(x \to \infty) = 0 \tag{58}$$

Mass consumption rate in the above equations is given as m = ρU, where U is the magnitude of the relative displacement velocity of the flame $\boldsymbol{U}$. For a premixed flame, it is equal to laminar burning velocity $s_L\boldsymbol{n}$ which is usually associated with the velocity at which the premixed flame will propagate into the unburnt mixture, given there is no fluid velocity. In figure 4, we can see that the flame front velocity is equal to zero, which means that the laminar flame speed s_L is exactly compensating the flow speed u_1. Laminar burning velocity is also a measure of the amount of fuel and oxidiser which is converted into products, by means of the mass consumption rate, which is defined as m = ρs_L.

2.3.2 Laminar Diffusion Flamelet

In the case of counterflow diffusion flamelets, a jet of fuel impinges on an oxidiser/air jet forming a flat stagnation plane with a flat diffusion flame at or close to stoichiometric plane. Since the flame is considered to be flat, the state variables h, ρ, Y_i are functions of x-coordinate (which is perpendicular to the flame surface) and time. x-component of gas velocity is a function of x-coordinate and time. y-component of gas velocity is a function of both x and y coordinates along with time. To take into account this flow in y-direction, we introduce a local flame stretch rate G(x,t) = $\dfrac{\partial v}{\partial y}$ and is a function of x-coordinate and time only. For steady counterflow flames, this equals to mass based stretch rate K. Profile for flame stretch rate is still unknown, but we can bring in the transport equation for local stretch rate G which is defined as above. Using the definition of flame stretch rate in 2, the equation reduces to

$$\frac{\partial \rho}{\partial t} + \frac{\partial (\rho u)}{\partial x} = -\rho G \tag{59}$$

This is because, as mentioned earlier, ρ is only a function of x coordinate and time. For unknown flamelet stretch field, transport equation can be derived from momentum equation in y direction. Detailed mathematical derivation is presented in appendix A of [22]. The equation is

$$\rho\frac{\partial G}{\partial t} + \rho u\frac{\partial G}{\partial x} = \frac{\partial}{\partial x}(\mu\frac{\partial G}{\partial x}) + P(t) - \rho G^2 \tag{60}$$

where P(t) denotes pressure gradient in y-direction. In far field, the flow is assumed to be potential flow. In oxidiser stream, velocity gradient can be prescribed which only depends on time:

$$\frac{\partial u}{\partial x}(x \to \infty) = -\frac{\partial v}{\partial y} = -G = -a(t) \tag{61}$$

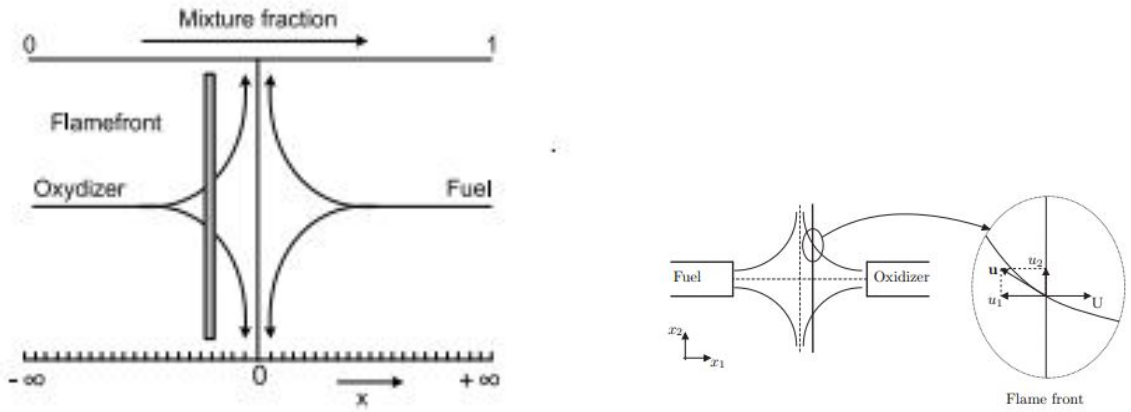

(a) (b)

Figure 5: Schematic Representation of non premixed flamelets (Source: [22] (left) and [6] (right))

In which a(t) is the applied strain rate which is only a function of time. We can obtain a(t) by substituting above equation in the equation before as:

$$P(t) = \rho_{ox}(\frac{\partial a(t)}{\partial t} + a(t)^2) \tag{62}$$

Thus, for unsteady counterflow diffusion flames, the set of flamelet equations can be written as:

$$\frac{\partial \rho}{\partial t} + \frac{\partial \rho u}{\partial x} = -\rho G \tag{63}$$

$$\frac{\partial(\rho Y_i)}{\partial t} + \frac{\partial \rho u Y_i}{\partial x} = \frac{\partial}{\partial x}(\frac{\lambda}{Le_i c_p}\frac{\partial Y_i}{\partial x}) + \dot{\omega}_i - \rho Y_i G, \quad i \in [1, N_s - 1] \tag{64}$$

$$\frac{\partial(\rho h)}{\partial t} + \frac{\partial \rho u h}{\partial x} = \frac{\partial}{\partial x}[\frac{\lambda}{c_p}\frac{\partial h}{\partial x} + \frac{\lambda}{c_p}\sum_{i=1}^{N_s}(\frac{1}{Le_i} - 1)h_i\frac{\partial Y_i}{\partial x}] - \rho h G \tag{65}$$

$$\rho\frac{\partial G}{\partial t} + \rho u\frac{\partial G}{\partial x} = \frac{\partial}{\partial x}(\mu\frac{\partial G}{\partial x}) + \rho_{ox}(\frac{\partial a(t)}{\partial t} + a(t)^2) - \rho G^2 \tag{66}$$

Dirichilet type boundary conditions are applied for enthalpy and species mass fraction

$$Y_i(x \to \infty) = Y_{i,ox}, \qquad h(x \to \infty) = h_{ox} \tag{67}$$

$$Y_i(x \to -\infty) = Y_{i,fu}, \qquad h(x \to \infty) = h_f u \tag{68}$$

For G, a combination of Dirichilet and Neumann boundary conditions is imposed.

$$G(x \to \infty) = a(t), \qquad \frac{\partial G}{\partial x}(x \to -\infty) = 0 \tag{69}$$

Parameter of this system is the applied strain rate defined at the oxidiser side. A series of flamelets are calculated by varying the values of applied strain rate in order to generate the

lookup table for $a \leq a_{ext}$, where a_{ext} denotes the extinction strain rate. For counterflow diffusion flames, mass burning rate can be considered to represent the amount of mass per unit areas that is converted into flame each second [6]. Velocity component in y direction $\boldsymbol{u_2}$ as shown in the figure accounts for the stretch. This local stretch rate acts as negative source term for the counterflow diffusion flames. Mass consumption rate, thus not only depends on the local composition and enthalpy, but also on the local stretching of the flow. The amount of mass of fuel $m_{F,1} = mY_{F,1}$ enters the domain through the inlet at x_1 = -L. It is partially converted into products and is partially leaked due to flame stretching.

$$m_{F,1} = -\int_{-L}^{L} (\dot{\omega_F} - \rho K Y_F) dx_1 \tag{70}$$

$$m = \frac{1}{Y_{F,1}} \int_{-L}^{L} (\dot{\omega_F} - \rho K Y_F) dx_1 \tag{71}$$

3 From Flamelet Equations to Manifold

What is a Manifold? What is its significance? [25]

The fundamental concept of generating reduced manifold by solving the flamelet equations and describing the solution thus obtained as explicit functions of control variables is based on Intrinsic Low Dimensional Manifold Method (ILDM) given by Maas and Pope [25]. Flamelet equations are solved to obtain a trajectory in the composition space, which depicts the chemical reactions taking place within the system. This solution gives us an idea about the details of the internal structure of the flame. The main fundamental difference between ILDM and FGM is that, FGM takes into account the effects of diffusion and convection, which is neglected by ILDM. This shows that, the chemistry happening within the system at lower temperatures, which could not be captured correctly by ILDM is now captured correctly by FGM. This is because the effects of diffusion and convection are not negligible as compared to the source terms at lower temperatures. We will understand in brief what do these manifolds represent and how are they generated.

State of a system involving chemical reactions can be described based on the set of partial differential equations (also known as conservation equations), which describe time dependent development of all the properties that determine the state of the system. At any time t, homogeneous system can be completely determined by a set of state variables, namely the enthalpy, the pressure and N_s composition variables, related to N_s species within the system, i.e. state of the system at any time can be represented as a point in N_s+2 dimensional space, also known as state space. If pressure and enthalpy are assumed to be constant, the state of the system can be represented as a point in N_s dimensional space, known as the composition space. Solution of conservation equations tells about the evolution of system involving chemical reactions in the form of a trajectory of this system in the state space. We can have three different choices of basis to describe the state space: the first one is vector of specific mole number for each species, the second one being the element composition vector

(which is the vector of number of atoms of an element in a particular species, total elements being N_e) and the third one being a set of linearly independent reaction vectors (which is the vector of stoichiometric coefficients of all the species for a particular reaction).For all elements j and reactions i, the reaction vector and element composition vector are orthogonal to each other.

Trajectory describing the chemical reactions taking place within the system is a part of the subspace of this state space which is known as Reaction Space (dimensionality $N_r = N_s$ - N_e). This reaction space is spanned by reaction vectors mentioned above. The realisable region within the state space is given by:

$$T(h, P, \phi) > 0 \qquad \text{(boundedness of temperature)} \tag{72}$$

$$P > 0 \qquad \text{boundedness of Pressure} \tag{73}$$

$$0 \leq M_i \phi_i \leq 1 \qquad \text{(boundedness of mass fraction)} \tag{74}$$

$$\sum_{1=1}^{N_s} w_i = \sum_{i=1}^{N_s} M_i \phi_i \qquad \text{(normalisation)} \tag{75}$$

The last constraint reduces the dimension of realisable subspace to N_s - 1, manifold M. Previous equation restricts the realisable compositions to a simplexS_ϕ in state space. Thus the combination reduces the realisable compositions to the intersection of M and S_ϕ, a $N_s - 1$ dimensional simplex. The significance of the realisable manifold in N_r dimensional subspace is that, if a system has state corresponding to a point on this manifold, for all times, the state of the system can be given by a point, which is also a point on this manifold. All the movements in the state space according to the linear combination of reaction vectors corresponds in change of state corresponding to the chemical reaction, which is, in other words, movement parallel to the manifold. Movement in the direction normal to this manifold (for homogeneous systems) is not allowed because it corresponds to a change of the elemental composition and also to the direction of element vectors (because, as mentioned earlier, element vectors and composition vectors are orthogonal to each other). Trajectories do not cross each other in the state space, and finally approach to one common point corresponding to the equilibrium condition.

We can visualise this by looking at a simpler example for a $O_3/O_2/O$ system [25]. We have a three dimensional composition space as shown in figure 6. The composition can be given by $\boldsymbol{\phi} = (\phi_{O_3}, \phi_{O_2}, \phi_O)$. Due to element conservation, we only have 1 element in this case. Thus possible states of the system are confined to a reaction subspace, which is a triangular plane given by the equation

$$M_{O_3}\phi_{O_3} + M_{O_2}\phi_{O_2} + M_O\phi_O = 1 \tag{76}$$

Within this triangle reaction takes place. Sample trajectory representing chemical reaction taking place within the system can be shown in the figure 6. The reaction space can be spanned by any two linearly independent reaction vectors. Equilibrium corresponds to one point in the composition space here, which is a zero dimensional subspace of the composition space.

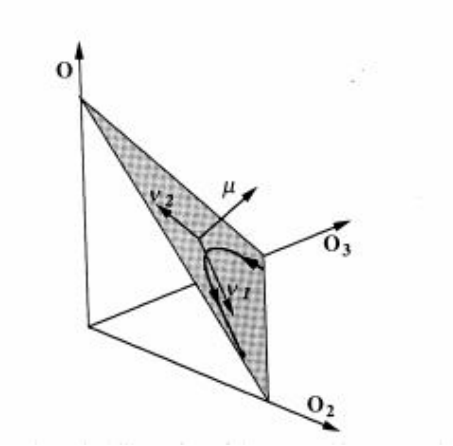

Figure 6: Schematic illustration os composition for a simple $O_3/O_2/O$ system (SourceJ. U.Maas, S.B.Pope,Simplifying chemical kinetics: Intrinsic low-dimensional manifolds in composition space, Combustion and Flame, Volume 88, Issues 3–4, March 1992, Pages 239-264.)

It is difficult ot visualise the solution in N_s dimensional composition space. Hence, we have shown projection of manifold in the figure 7. We can find one notable feature that the trajectories try to approach and bunch towards each other long before equilibrium is attained. It looks like there is a presence of a lower dimensional manifold within the reaction subspace that has the property that all trajectories tend to approach the manifold and on this manifold, only slow time scales govern the chemical reactions. Systems with initial conditions which do not lie on this manifold evolve rapidly to approach the manifold initially and finally evolve in the direction of the manifold. This is done by defining $N_c(= N_r - N_f)$ dimensional manifold within the reaction subspace by the condition that components in the direction of N_f distinct basis vectors vanish (in other words, component of velocity vectors in the direction of eigenvectors corresponding to N_f most negative eigen values vanish). Only restriction imposed in the method is the choice of the dimension N_c of the manifold in the reaction subspace. This value of dimension of the manifold usually provides the number of parameters with respect to which the manifold obtained in the reaction subspace can be parameterised. Figure 8 gives a visualisation of how the states corresponding to large negative eigen values approach the manifold which has lower values of velocity and finally evolution in time takes place along this manifold which is governed by slower time scales.

Thus, we have seen that how the tabulation of manifold as a function of a few parameters reduces the dimension of the composition space remarkably. This is very much helpful to perform pdf calculations for complex reacting turbulent flows, where the dimension of the composition space determines the number of transport equations to be solved in addition to continuity and the momentum equation. The method itself gives knowledge about the chemistry. Together with the construction of lower dimensional manifold, information about characteristic time scales (eigen values) and corresponding characteristic directions (eigen vectors) is obtained. Thus having the knowledge of physical time scales of the combustion process considered (e.g. diffusion, turbulent time scales), we can decouple those fast time scales that are much faster than the physical time scales in the systems. The reaction

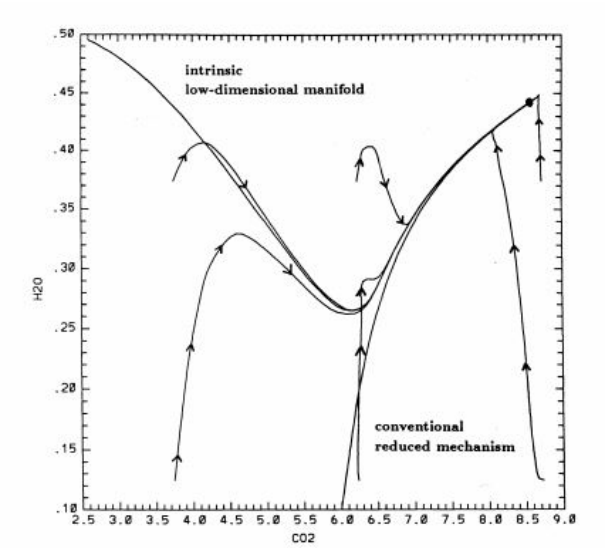

(a) 1 Dimensional Manifold

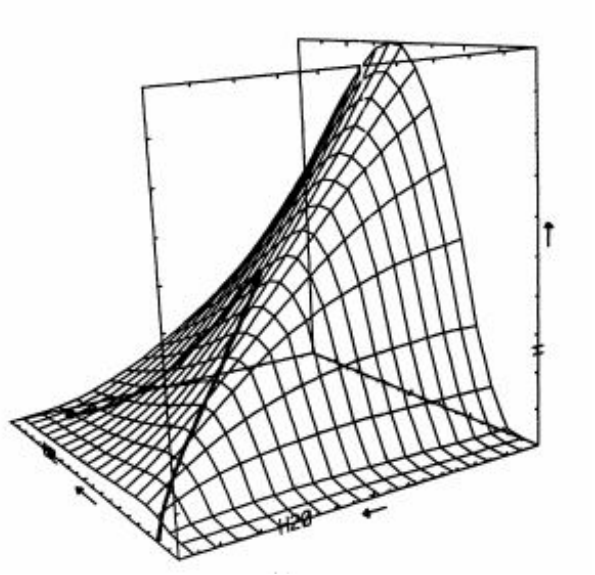

(b) 2 Dimensional Manifold

Figure 7: Plot of 1 dimensional manifold for specific mole number of H_2O along with sample trajectories (left) and plot of 2 Dimensional manifold for the specific mole number of H (Source: Source:U.Maas, S.B.Pope,Simplifying chemical kinetics: Intrinsic low-dimensional manifolds in composition space, Combustion and Flame, Volume 88, Issues 3–4, March 1992, Pages 239-264.)

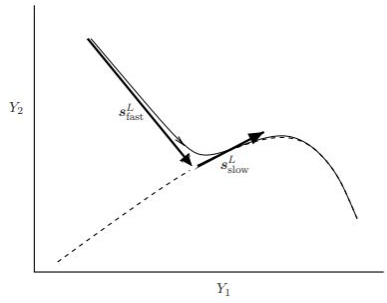

Figure 8: Fast and slow reaction processes in composition space. The reaction path (solid line) is attracted towards the manifold (dashed line) (SourceJ. A. van Oijen, Flamelet-generated manifolds : development and application to premixed laminar flames, Eindhoven: Technische Universiteit Eindhoven.)

space is parameterised only in terms of the few state variables, hence helping t reduce the dimension of composition space globally. For given values of these controlling variables, values of other state variables are explicitly given by the functions which parameterise other state variables in terms of controlling variables. These results are then used to calculate temporal development of the chemical states which is used by a table lookup as in the pdf methods used to perform turbulence simulations. It has been found that the cost involved with this generation of lookup table for low dimensional manifold and integrating it further

with the flow solver is greatly reduced as compared to solving transport equations for species, enthalpy separately. Choice of parameterising variables does not affect construction of the manifold, it only affects the way of mapping.

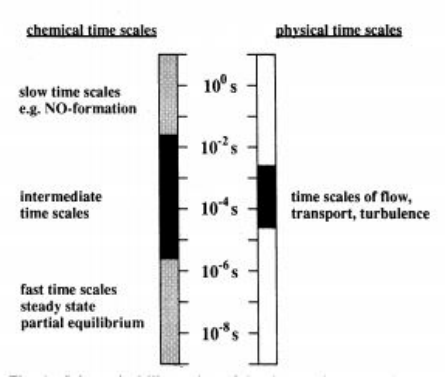

Figure 9: Schematic illustration of time scales governing a chemically reacting flow (Source:U.Maas, S.B.Pope,Simplifying chemical kinetics: Intrinsic low-dimensional manifolds in composition space, Combustion and Flame, Volume 88, Issues 3–4, March 1992, Pages 239-264.)

4 Coupling with flow solver [15]

After the manifold is stored in the form of a lookup table after paramterisation of solution of flamelet equations by a controlling variable, it can be linked to a standard CFD code [6, 14, 15]. First, in the initialisation phase, the database is stored into the memory. Then transport equations are solved for the controlling variables by the CFD solver along with continuity and momentum equation as shown in figure 1. Transport equations for the controlling variables can be derived by taking proper linear combinations of the original species equations 4. For the progress variable defined as $y = \sum_{i=1}^{N_s} \alpha_i Y_i$, we can write:

$$\frac{\partial}{\partial t}(\rho \sum_{i=1}^{N_s} \alpha_i Y_i) + \nabla \cdot (\rho \boldsymbol{v} \sum_{i=1}^{N_s} \alpha_i Y_i) = \nabla \cdot (\frac{\lambda}{c_p} \sum_{i=1}^{N_s} \frac{\alpha_i}{Le_i} \nabla Y_i) + \sum_{i=1}^{N_s} \alpha_i \dot{\omega}_i \tag{77}$$

which can be re written as

$$\frac{\partial}{\partial t}(\rho y) + \nabla \cdot (\rho \boldsymbol{v} y) - \nabla \cdot (\frac{\lambda}{c_p} \nabla y) = \nabla \cdot (\frac{\lambda}{C_p} \sum_{i=1}^{N_s} \alpha_i (\frac{1}{Le_i} - 1) \nabla Y_i) + \dot{\omega}_y \tag{78}$$

where $\dot{\omega}_y$ is the progress variable source term which is given by

$$\dot{\omega}_y = \sum_{i=1}^{N_s} \alpha_i \dot{\omega}_i \tag{79}$$

The first term in RHS of 78 represents fluxes due to preferential diffusion. This term is equal to zero in case of unity Lewis numbers. It is assumed that the gradients of control variables ∇y_i is not independent but correlated as in 1 D flamelets as $\nabla y_i = c_i \nabla y$, with c_i being a function of control variables. Thus, the transport equation can now be re written as:

$$\frac{\partial}{\partial t}(\rho y) + \nabla \cdot (\rho \boldsymbol{v} y) - \nabla \cdot (\frac{\lambda}{c_p} \nabla y) = \nabla \cdot (D_y \nabla y) + \dot{\omega_y} \tag{80}$$

The preferential diffusion coefficient D_y is stored in the FGM table. In similar way, we can derive transport equation for different control variables. In case of problems involving heat loss, enthalpy is regarded as to be additional control variable and the transport equation can be written as:

$$\frac{\partial}{\partial t}(\rho h) + \nabla \cdot (\rho \boldsymbol{v} h) - \nabla \cdot (\frac{\lambda}{c_p} \nabla h) = \nabla \cdot (D_h \nabla y) \tag{81}$$

with D_h as the preferential diffusion coefficient.

Thus as mentioned at the beginning of this section, transport equations for control variables are solved during the run time together with the momentum and the continuity equation and all the inputs required for this simulation i.e. $\rho, c_p, \lambda, \dot{\omega_y}, D_y, D_h, T$ are retrieved from the database. Since progress variable for adiabatic flows is a linear combination of mass fractions, the boundary conditions for y are straightforward to implement and follow the definition $y = \sum_{i=1}^{N_s} \alpha_i Y_i$. In case of non-adiabatic flows, as mentioned before, enthalpy is an additional control variable whose transport equation is to be solved during the flow simulation. Boundary conditions for h are cumbersome because they are not mentioned in terms of enthaply bt are mentioned in terms of temperature at the boundary. Thus an iterative procedure may be needed to obtain enthalpy at the boundary. An alternative to this is that h_{wall}, which is a function of T_{wall} is solved as a pre-processing step for a given T_{wall} and stored in the lookup table as a function of progress variable y. The species mass fractions are retrieved from the database during the post processing step and is not required to solve transport equations for them.

With this, we have come to an end to understand what is Flamelet Generated Manifold method, what is theory on which the model is based, derivation of the equations which define the model and how the implementation of model can be performed to solve problems associated with combustion. Now from next section, we will have a review of how this method was applied by different groups to solve combustion problems and what are the results and conclusions obtained.

5 Applications

We will try to understand more about Flamelet Generated Manifold method by looking at some cases where the method was used by gropus around the world to solve problems related to Combustion.

5.1 Premixed Laminar Flames

5.1.1 1 D Burner Stabilised Flame

First and foremost, the method was used by van Oijen to study freely propagating flat flame (one dimensional burner stabilised flame) containing methane/air mixture [14]. FGM method was compared with detailed chemical mechanism which consisted of 16 species and 25 reversible reactions. As the burner stabilised flames are subject to non-adiabatic effects due to heat losses to the burner side, transport equation of enthalpy was solved along with the transport equation for the progress variable. Burner outflow was positioned at x = 0 and for x < 0, the burner area was kept constant at a temperature of 300 K. Stationary solutions were constructed for mass flow rates ranging from 0.05 to 0.50 kg/m^2s. Flames were computed using CHEM1D flame solver developed at Eindhoven University of Technology. In the figure 10, profiles of controlling variables Y_{O_2} and h are shown along with profiles of Y_{CH_2O} and Y_H. Here Y_{O_2} is the progress variable which indicates the progress of chemical reaction as the value changes monotonically. The profiles calculated using FGM matched quite well with the results obtained using detailed chemistry.

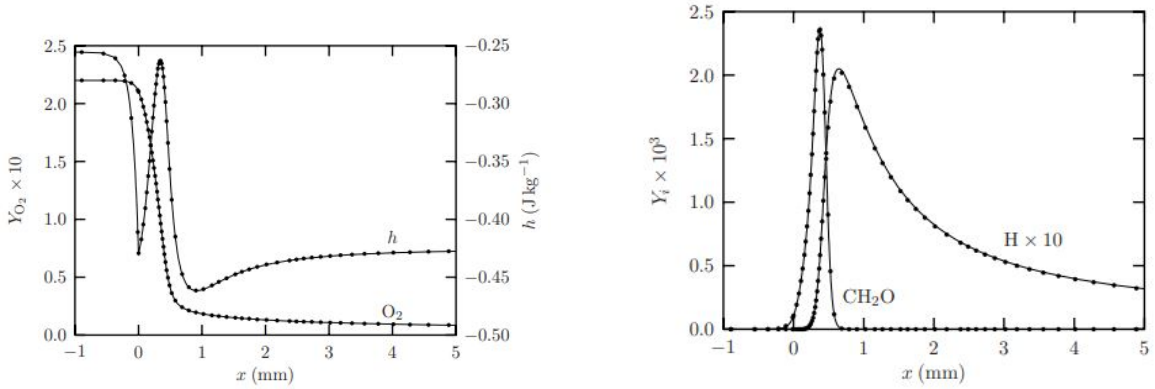

(a) (b)

Figure 10: Profiles of Y_{O_2}, h in fig (a), Y_{CH_2O}, Y_H in figure (b) for 1-d Burner Stabilised Flame, Line: experiment, symbols: FGM. m = 0.30 kg $m^{-2}s^{-1}$(Source: J. A. van Oijen,,Flamelet-generated manifolds : development and application to premixed laminar flames,Eindhoven: Technische Universiteit Eindhoven.)

5.1.2 2 D Burner Stabilised Laminar Flame

Next, he also performed calculation of a 2-D burner stabilised laminar premixed flame [14], where methane/air flame flame with an equivalence ratio of $\phi = 0.9$ was stabilised on a 2D slot burner in a box. The burner was 6mm wide while the box was 24 mm wide. Burner walls and box walls were kept at 300 K, velocity profile is parabolic with maximum velocity

equal to 1 m/s. Results of the calculations are compared with detailed chemistry and are shown in the figure 11.

Iso-contours of T and mass fractions of CO, O_2, H are shown. Results obtained using FGM match quite well with the detailed chemistry computations. Position of the flame is predicted very well and also the mass fraction are reproduced well. Flame cooling governing the stabilisation of the flame on the burner is captured well using FGM. There are some differences in contours of Y_{CO} near the burner walls, where the contours do not attach with the walls in FGM calculations. Y_{CO} follows from FGM database where diffusion along the flame front is not considered and hence the mass fraction of CO is under predicted in this area which is dominated by diffusion. To take this into account, we should consider a higher dimensional manifold.

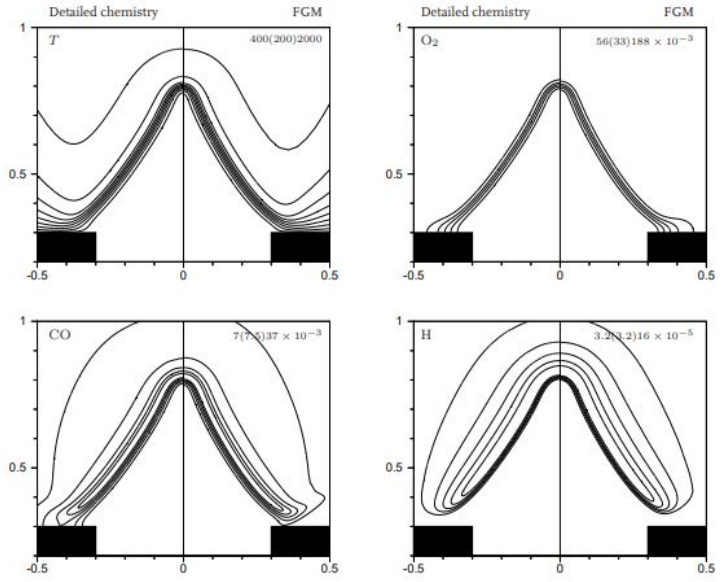

Figure 11: Isocontours of T, mass fractions of CO, O_2, H computed using detailed chemistry (left) and FGM (right). Space coordinates are given in cm.(Source: J. A. van Oijen,,Flamelet-generated manifolds : development and application to premixed laminar flames,Eindhoven: Technische Universiteit Eindhoven.)

5.2 Sandia Flames C, D, E and F

Lookup tables were prepared for archetypal flamelets: laminar, premixed, stretchless adiabatic flames and counterflow planar diffusion flames [22].These tables were then used to study Sandia Flames C, D, E and F to see which of the archetypal flames represent the practical combustion case in a better manner. This is because, most of the combustion problems we encounter in practice are partially mixed in nature. In Sandia Flames, we have main jet (diameter = 7.2 mm) and pilot surrounding the main jet (annulus inner diameter = 7.7

mm, outer diameter = 18.2 mm). Coflow velocity is equal to 0.9 m/s @ 291 K, 0.993 atm. Properties of main jet are: composition: 25% CH_4, 75% dry air by volume, viscosity = 1.58 e-05 m^2/s. Main jet velocity @ 294 K, 0.993 atm: $U_C = 29.7m/s, U_D = 49.6m/s, U_E = 74.4m/s, U_F = 99.2m/s$. Simulations were performed and measurements were taken at dif-

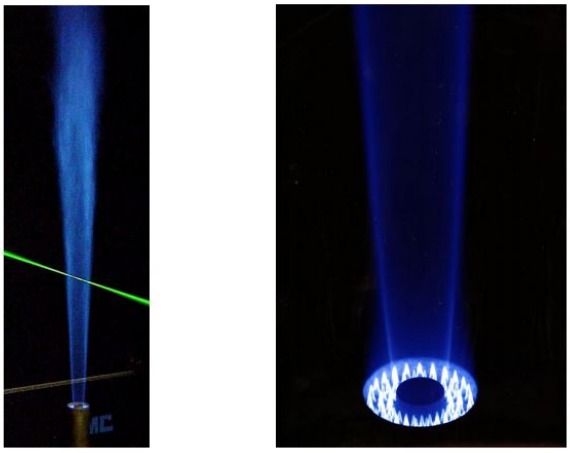

Figure 12: Sandia Flame D (left) with Nd: YAG laser beam and close up of the pilot flame (right)(Source: Robert Barlow and Jonathan Frank Piloted CH4/Air Flames C, D, E, and F – Release 2.1, Sandia National Laboratories, https://www.sandia.gov/TNF/DataArch/FlameD.html .)

ferent locations on the axis of the burner and at different directions in the radial direction as well. Simulations were performed using premixed and non-premixed flamelets for unity and non unity Lewis numbers.

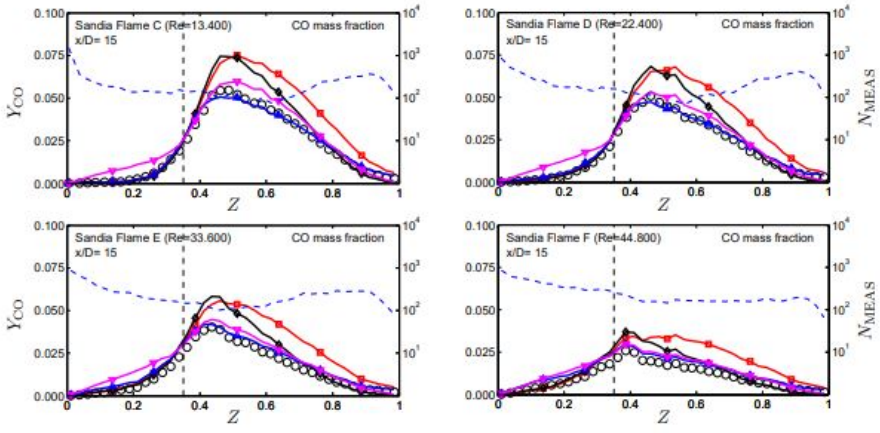

Figure 13: Averaged conditional CO mass fractions in Sandia Flame C, D, E and F at x=15D. Symbols identical to those in figure 14 have been used.(Source: Ramaekers, W. J. S., Development of flamelet generated manifolds for partially-premixed flame simulations, Eindhoven: Technische Universiteit Eindhoven.)

In figures 14 and 13 we can say that the simulation results obtained by using premixed flamelets are more representative of the flow for Sandia Flames. Results with unity and non unity Lewis numbers are in close conjuction with each other. Detailed explanation of results and conclusions can be found in [22].

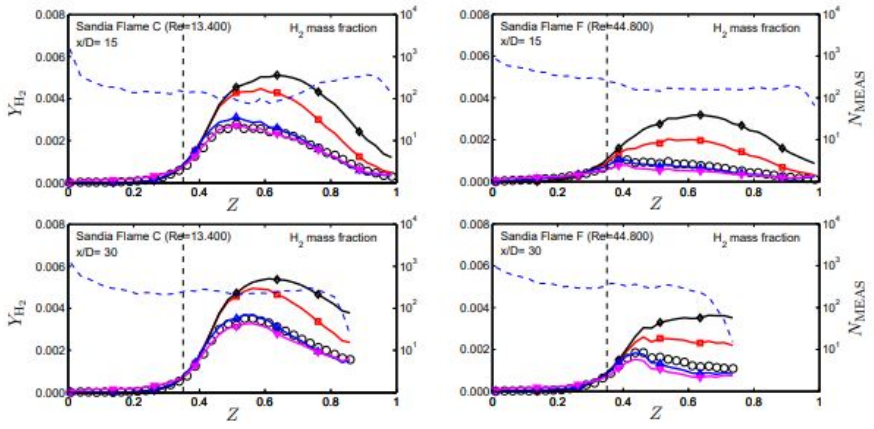

Figure 14: Averaged conditional H2 mass fractions in Sandia Flame C and F at x=15D and 30D. Black circles denote measurements, red lines with square markers denote predictions from the FGM-PL, black lines with diamond markers denote predictions from the FGM-PC, blue lines with upwards directing triangle markers denote predictions from the FGM-DL and magenta lines with downwards directing triangle markers denote predictions from the FGM-DC. The blue dashed line represents the number of measurements per Z-bin; values are stated on the right y-axis. The vertical black dashed line indicates the stoichiometric mixture fraction.(Source: Ramaekers, W. J. S., Development of flamelet generated manifolds for partially-premixed flame simulations, Eindhoven: Technische Universiteit Eindhoven.)

5.3 Laminar Non Premixed Coflow Flames

Ability of FGM approach for numerical simulation of multidimensional laminar non-premixed flames was studied by Verhoeven et al [16]. Here, manifolds were constructed using both premixed and non premixed one dimensional flamelets, to methane flame in the co-flow of air. In the study, methane/air co-flow diffusion flame is considered. The burner is formed by two concentric tubes where the fuel flow contains 55 mol% of methane and 45 mol% nitrogen. Fuel tube diameter is 0.012 m. The co-flow of air had an outer diameter of 0.055 m. Stochiometric mixture fraction = 0.124. Both oxidiser and fuel entered the geometry with a temperature of 300 K. Fuel velocity was modeled using parabolic profile with maximum velocity equal to 0.23 m/s and co-flow air was modeled by plug flow with constant velocity equal to maximum velocity of the fuel inlet. No slip boundary condition was applied at the walls. Plots of Temperature, CO, OH mass fractions were plotted radially at heights 0.01 m, 0.04 m, 0.08 m for unity Lewis numbers and non Lewis numbers with detailed chemistry, premixed and non-premixed flamelets. It can be seen that non-premixed FGM matches the detailed chemistry in a better sense as compared to premixed FGM model. For detailed

results of the study performed, please refer [16]

5.4 Stratified Premixed Cooled Flames

Donini et al. studied the combined effects of heat loss and stratification in the FGM context[9]. Cooled stratified premixed methane/air flames are considered at atmospheric pressure conditions. FGM consists of a 3-D manifold where the control variables are represented by the progress variable (y), enthalpy (h) and mixture fraction (Z). Flamelets are calculated as steady, laminar, fully premixed flat flames for a given pressure, composition and temperature of the given mixture. Unity Lewis Number is imposed along the flamelets neglecting diffusion effects. Flamelet equations were solved using CHEM 1D solver in which chemistry was represented by GRI-Mech 3.0 mechanism consisting of 325 elementary reactions and 53 species with hydrocarbons upto propane. 6mm wide burner was present and parabolic profile was assumed for incoming mixture with maximum velocity being equal to 1 m/s. Results obtained using FGM were compared with results obtained using detailed chemistry. Results of temperature and mass fractions of OH were in excellent agreement with each other. Exception was small region near the burner where flame stabilises, which showed incorrect predictions of CO mass fractions. To take this into account, extra transport equation should be solved for keeping track of CO by adding a control variable.

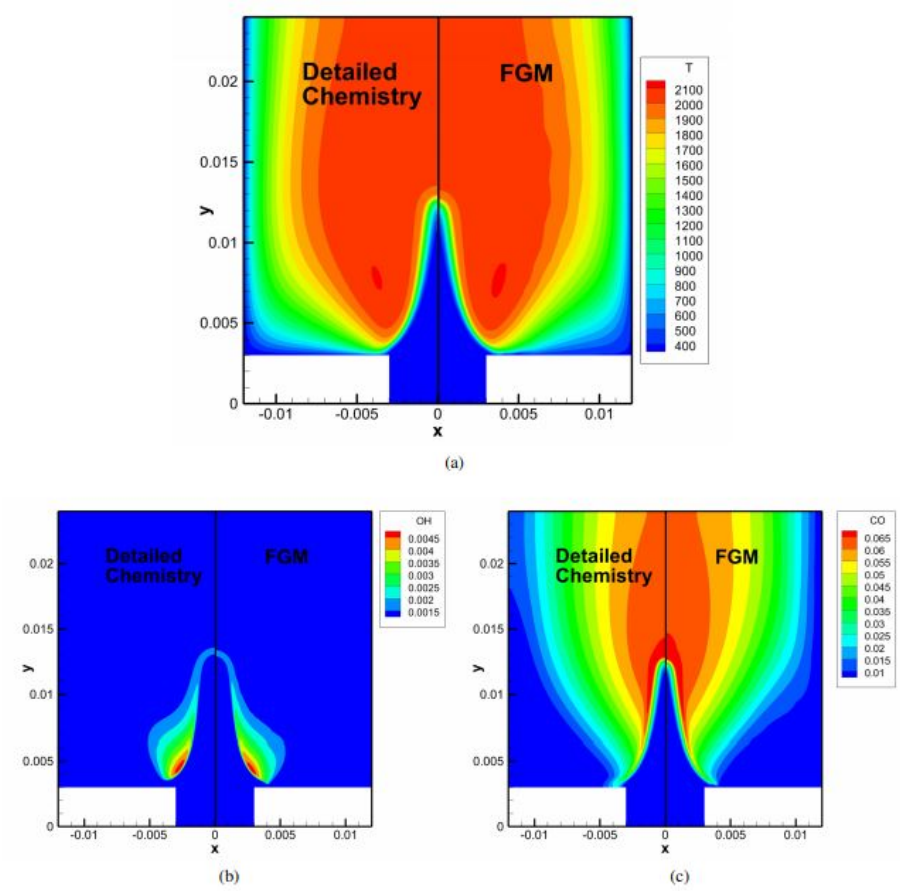

Figure 15: Isocontours of T [K], mass fractions of CO, OH computed using detailed chemistry (left) and FGM (right). Space coordinates are given in m.(Source: [9])

5.5 Gas Turbine Modeling

FGM was used to reduce chemistry to perform computational analysis of a confined premixed turbulent methane/air jet flame and fluid flow was modeled in RANS context [8]. Heat loss was described by selecting enthalpy as an additional progress variable and solving additional transport equation for it. Generic lab scale burner was used by the authors for high-velocity preheated jets for validation of the computation results. Brief description of the burner is as follows: Burner consists of a rectangular refinement with an off-center positioning of the jet nozzle enabling flame stabilization by recirculation of hot combustion products. The inlet speed is appropriately high, in order to be close to the blow out limit. The objective of this research was to simulate turbulent jet flame in high Reynolds number flow conditions, relevant to the gas turbine domain. Chemistry was represented by the GRImech 3.0 mechanism which consisted of 325 elementary reactions between 53 species with hydrocarbons upto propane. Unity Lewis Number assumption was chosen for the calculation of flamelets. Ansys-SFX 14.0 was used to solve the flow problem and it was coupled with three dimensional FGM implementation.Inlet conditions were as follows: velocity = 90 m/s, temperature

= 593 K, premixed methane/air equivalence ratio = 0.71, atmospheric conditions, parabolic inlet velocity profile to account for the presence of walls.Following figure shows the overview of the profile and behaviour of the combusting flow in the burner. The presence of a vast recirculation zone is noticable at the side of the nozzle exit, which flanks almost entire jet. In this large scale recirculation zone, hot products of combustion are carried back to the inlet, enhancing ignition of the fresh incoming gases.

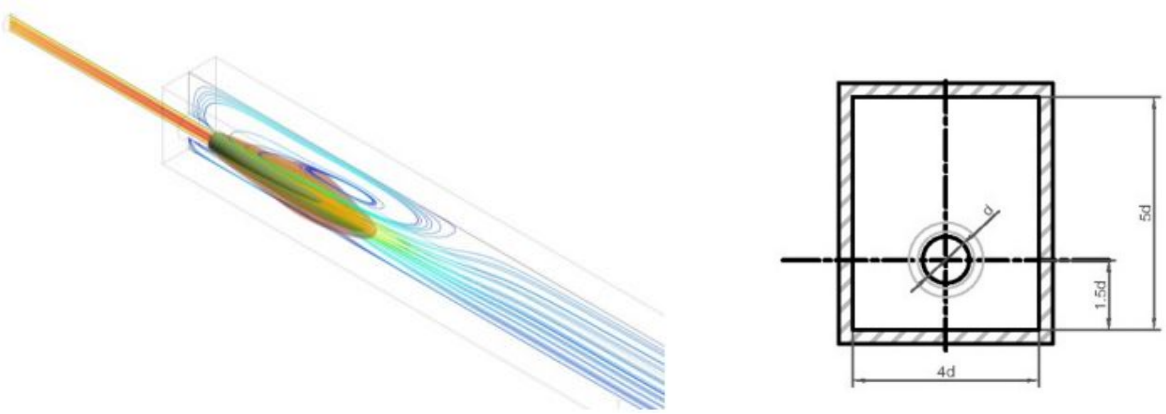

(a) (b)

Figure 16: Schematic view of results of velocity streamlines at the centre plane colured as a function of velocity in fig (a) and transverse cross section of the combustor in fig (b) (Source: Donini, A., Martin, S. M., Bastiaans, R. J. M., van Oijen, J. A., and de Goey, L. P. H.,Simulations of a Premixed Turbulent Confined Jet Flame Using the Flamelet Generated Manifold Approach With Heat Loss Inclusion, Proceedings of the ASME Turbo Expo 2013)

Comparison of this computation including heat loss was done with experimental data by the authors. Also comparison was made with model which does not take into account the heat loss, which thus had two dimensional implementation of the FGM. Results of axial velocity and temperature at locations 2d, 10d and 15 d are presented in figure 17. Measurements were taken at different lines at a cross section which is shown in the figure 16.

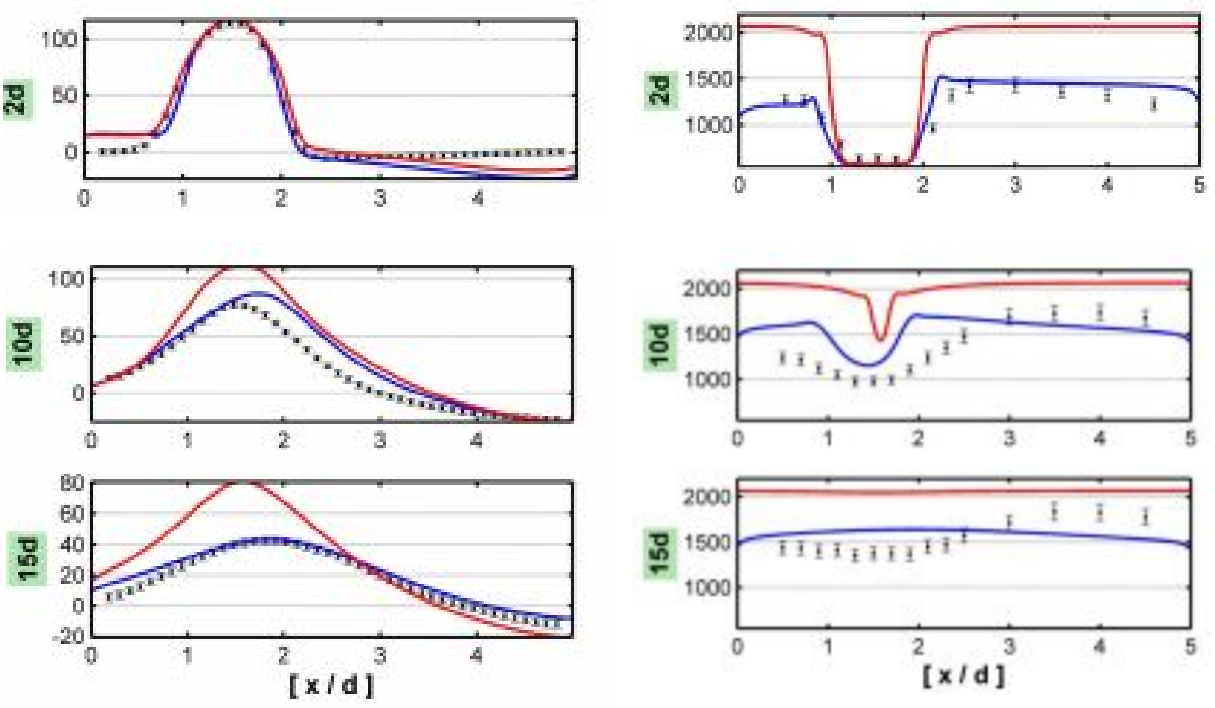

(c) Axial Velocity (d) Temperature

Figure 17: Axial velocity and Temperature at locations 2d, 10d and 15d along the axis of the combustor. (Source: Donini, A., Martin, S. M., Bastiaans, R. J. M., van Oijen, J. A., and de Goey, L. P. H.,Simulations of a Premixed Turbulent Confined Jet Flame Using the Flamelet Generated Manifold Approach With Heat Loss Inclusion, Proceedings of the ASME Turbo Expo 2013)

We can see that the method captures combustion features quite well, leading to a representative prediction of the profiles of velocity and temperature. There is some mismatch between experimental and computational results which was accounted to the partially incorrect prediction of the recirculation region extension along the burner. The effect of recirculation zone is quite significant in this burner. This is because, the burnt gases lose heat to the walls with low velocities and hence enhanced heat exchange. The inlet jet is adjecent to this region and this eventually leads to low igniting temperature of the flame. Hence to capture the entire combustion process correctly, it is extremely important to obtain a better model for the recirculation zone. Even though the flow modeling was a bit poor, combustion features in the gas turbine could be reproduced with a reasonable computational effort using FGM reduced chemistry. For more detailed results please refer [8].

5.6 IC Engines

In recent times, FGM has also been applied in few cases to study combustion in diesel and gasoline IC engines. A brief discussion on the results obtained for IC engines is mentioned

below.

5.6.1 CI Engines

Maghbouli et al. [2] studied combustion within compression ignition engines by incorporation of FGM combustion closure. Simulations were performed using OpenFOAM. FGM lookup tables for counterflow diffusive flame configurations were generated. Chem1D code was used to solve the flamelet equations. n-dodecane was used as a fuel for the IC engine. Specifications of Sandia Engine are given in table 9 of [2]. Simulation results obtained using FGM reduction method for flame lift-off, in-cylinder pressure and average heat release rate were compared with the results obtained with the experiments for two cases of High temperature Short Ignition Delay (HT-Sh-ID) and High Temperature Long Ignition Delay (HT-Lo-ID).It was concluded that FGM closure was capable of accurate predictions for non/partially premixed configuration under a variety of operating conditions. Few other cases where FGM was applied to study combustion for within Compression Ignition IC engines are [21, 24].

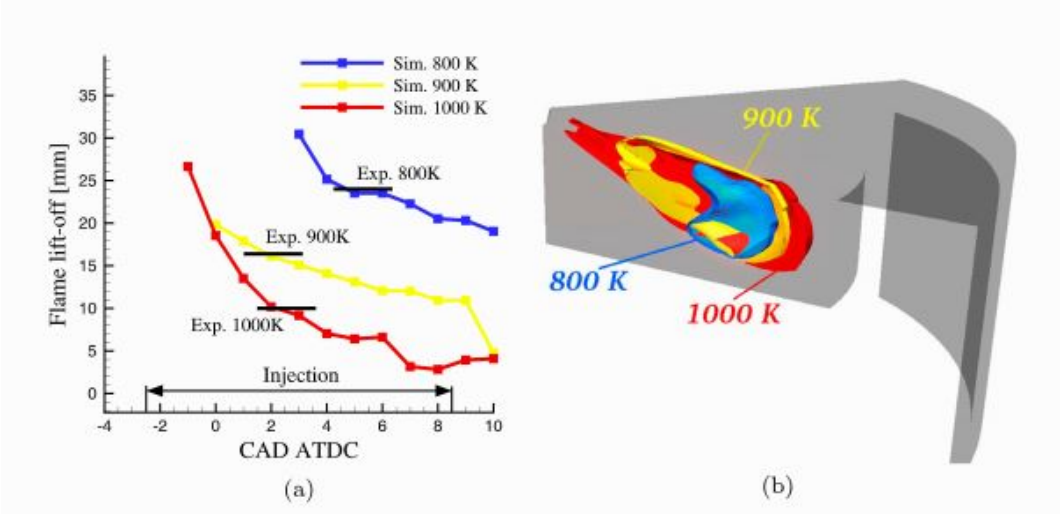

Figure 18: (a) Temporal results of flame lift-off for 800 K, 900 K, and 1000 K ambient temperatures compared with the mean experimental values. (b) Iso-surfaces 2% of the maximum OH as a marker of the diffusion flame at 5 CAD ATDC for targeted ambient temperatures (Source: [2])

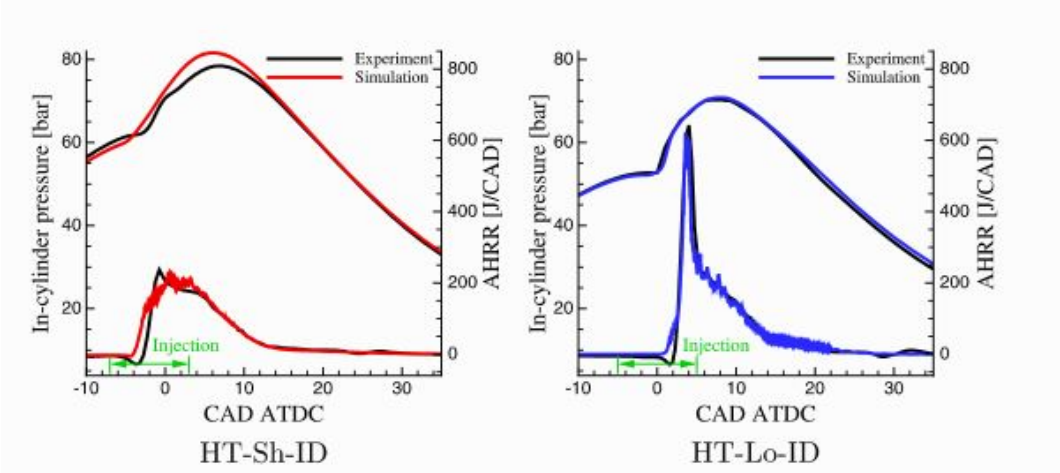

Figure 19: In-cylinder pressure and AHRR of the HT-Sh-ID and HT-Lo-ID cases compared with the experiments (Source: [2])

5.6.2 SI Engines

Goryntsev et al. [11] performed numerical simulations to model SI Engine Combustion and Knock making use of tabulated chemistry generated using FGM. This was the first of its kind and the only study performed on SI engines till now, according to the author. AVL FIRE CFD software was used to predict the combustion and the knock probability in passenger car gasoline engine by applying the FGM combustion model. Simulation results were compared to the corresponding experimental data. Detailed chemistry was used to generate lookup tables using the AVL TABKIN table generation tool. FGM based knock model was used to predict knock within SI engine. It was finally inferred by the authors that FGM combustion model demonstrates potential of delivering a high level description of the combustion processes in gasoline engines and providing single chemistry model for detailed characterisation of combustion, knock emissions. Application of FGM to predict emissions was left as future work.

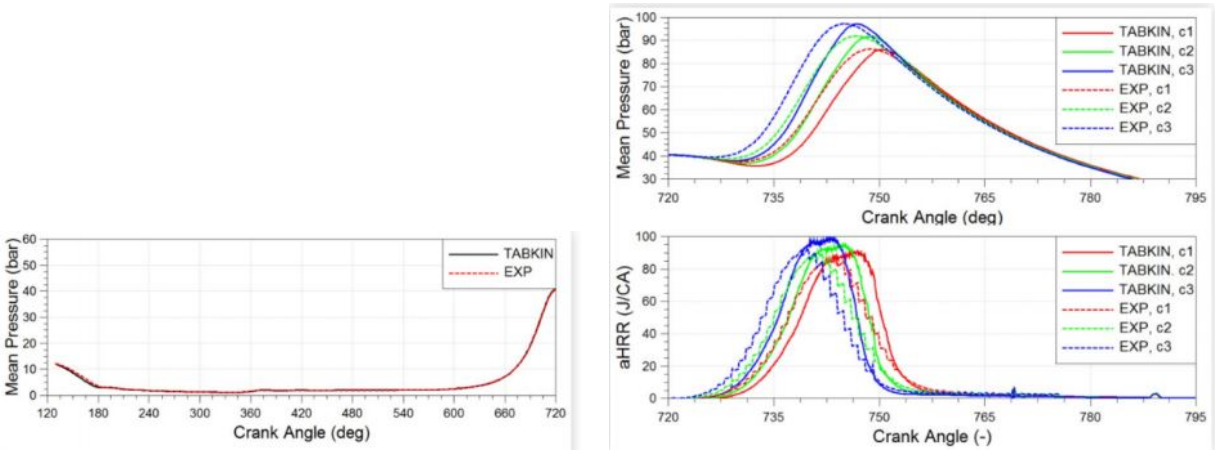

Figure 20: Simulated and measured in-cylinder pressure (left), in cylinder pressure curves (right - top) and apparent heat release rate (right - bottom) for spark timing sweep: FGM (solid lines), experimental mean pressure (dashed lines) (Source:Goryntsev, D., Tap, F., Tvrdojevic, M., and Priesching, P., "SI Engine Combustion and Knock Modelling Using Detailed Fuel Surrogate Models and Tabulated Chemistry," SAE Technical Paper 2019-01-0205, 2019)

FGM was also used in cases to model combustion of evaporating sprays [3, 12]. Thus we can see that application of FGM is quite wide spread and it is delivering quite satisfactory results in many cases.

6 Future Scope of Research

6.1 Definition of control variable

IN FGM reaction progress variable y is used to describe the progress of combustionan is generally used as the second controlling parameter to tabulate the manifold which is constructed from unsteady laminar flamelets. There are a few requirements which are to be met by the definition of this progress variable y. It should have a monotonic variation from a non reactive state of the mixture to the attainment of the steady state or completion of rection between the ideal gases. Usually, it is defined as linear combinations of mass fraction of reactive species present in the mixture. Ad-hoc formulation may not always give us optimal results. Lookup tables are generated for a step of values of the controlling variables. For determining values of state properties which lie in between, linear interpolation is used, which leads to some errors in values extracted. Some definitions of optimal progress variable was tried by Vasavan et al. to take care of both the issues which was adaptive in nature [1]. For details please refer [1]. He performed simulations using this new definition and compared results with detailed chemistry along with simulation results of two other definitions (which were some linear combinations of mass fraction of species) for 3 test cases. Results for ECN

spray-A using n-dodecane as fuel are shown below.

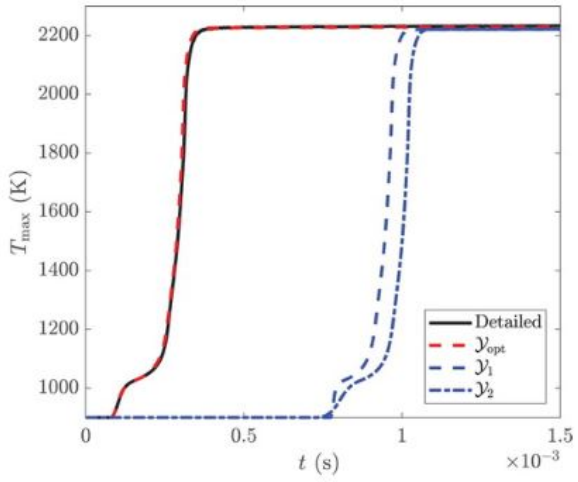

Figure 21: Comparison of maximum temperature for ECN Spray-A, with n-dodecane as fuel in an igniting counterflow flame configuration with detailed chemistry and FGM with multiple progress variable combinations. The strain rate is 100/s (colour online)(Source: Aromal Vasavan, Philip de Goey and Jeroen van Oijen (2020) A novel method to automate FGM progress variable with application to igniting combustion systems, Combustion Theory and Modelling, 24:2, 221-244)

Thus, definition of progress variable for FGM technique is a topic of active research along with methods to store the formulated table as well as to retrive data from the table when performing simulations.

6.2 Flamelet Lookup Table

Usually, when obtaining llokup table using FGM method, we need to select the type of flamelets based on which the table is to be generated. Most of the practical combustion problems in nature are partially premixed in nature. But the flamelets used are either premixed or non-premixed. Hence research can be done to improve FGM method in order to develop a generalised model which can be applied to most of the partially premixed applications. Goldin et al. [10] tried to stdy some generalised combustion model for partially premixed flames to estimate CO quenching in gas turbine combustors. But they finally cocluded that no single flamelet model can give required results. Hence more work can be done in this field.

6.3 NO_x predictions

In the papers read so far, no contours or plots have been plotted to predict amount of NO_x generated using FGM method. In the review paper [15], there is one section on NO

generation prediction using FGM method. In order to predict NO formation, two methods were used. In first one, NO mass fraction values were interpolated directly from the lookup table generated by solving detailed chemistry. In another method, explicit transport equation for NO was solved to track its production within the reacting space. But it is mentioned that mixed results were obtained, and no conclusive evidence can be obtained on how FGM fairs to predict NO production. Thus this can be looked at as a potential topic of future research related to FGM.

7 Learnings

Flamelet Generated Manifold helped to understand how problems related to Turbulent approach can be approached. Flamelet methods is one set of approach, which utilises iso-surfaces of progress variable y to locate flame in three dimensional space. Progress variable varies from its value from unburnt to burnt in premixed flames and flame to oxidiser in non-premixed flames. 3-dimensional turbulent flame can be considered as an ensemble of laminar one-dimensional flamelets according to flamelet models, in the flamelet regime. Evolution of flame in 3-dimensional space with time can be tracked by solving transport equation for the progress variable y or by solving kinematic equation of the progress variable y along with determining flame-speed at each point of time using some method. According to Intrinsic Low Dimensional Manifold method, chemical reactions taking place within the system can be seen as trajectory within the state space, which denotes evolution of state of the system with time. Vectors corresponding to most negative and zero eigen values can be considered to be in partial equilibrium and the trajectory can further be defined only by equations which are slow. Reaction subspace is a subspace of the state space in which the reaction trajectory is actually present. Solution obtained within the state space can be parameterised in terms of reduced number of variables to generate a lookup table, which in turn reduces the dimensionality of the state space. Number of transport equations to be solved in addition to continuity and momentum equals the number of variables with respect to which the solution within the state space is paramterised. Going through the literature review helped to develop an understanding of how the combustion problems are formulated using the Flamelet Generated Manifold method. Aslo some understanding related to experimental setups which can be used to mimic actual systems is obtained.

References

[1] Aromal Vasavan, Philip de Goey and Jeroen van Oijen *A novel method to automate FGM progress variable with application to igniting combustion systems* , Combustion Theory and Modelling, 2020, 24:2, 221-244, DOI: 10.1080/13647830.2019.1673902.

[2] Amin Maghbouli, Berşan Akkurt, Tommaso Lucchini, Gianluca D'Errico, Niels G. Deen, Bart Somers, *Modelling compression ignition engines by incorporation of the*

flamelet generated manifolds combustion closure , Combustion Theory and Modelling, 2019, 23:3, 414-438.

[3] Armin Wehrfritza, Ossi Kaario, Ville Vuorinen, Bart Somers, *Large Eddy Simulation of n-dodecane spray flames using Flamelet Generated Manifolds* , Combustion and Flame, Volume 167, May 2016, Pages 113-131.

[4] C.K. Law *Combustion Physics* , Cambridge University Publication, 2006

[5] Cardoso de Souza, T., Bastiaans, R. J. M., Geurts, B. J., and De Goey, L. P. H., *LES and RANS of Premixed Combustion in a Gas-Turbine Like Combustor Using the Flamelet Generated Manifold Approach.* ,Proceedings of the ASME 2011 Turbo Expo: Turbine Technical Conference and Exposition. Volume 2: Combustion, Fuels and Emissions, Parts A and B. Vancouver, British Columbia, Canada.

[6] Delhaye S., *Incorporating unsteady flow-field effects in flamelet-generated manifolds* , [Ph. D. thesis], Eindhoven University of Technology; 2009

[7] J. Warnatz, U. Maas, R. W. Dibble, *Combustion* , Springer Publication, 3rd Edition

[8] Donini, A., Martin, S. M., Bastiaans, R. J. M., van Oijen, J. A., and de Goey, L. P. H., *Simulations of a Premixed Turbulent Confined Jet Flame Using the Flamelet Generated Manifold Approach With Heat Loss Inclusion.* , Proceedings of the ASME Turbo Expo 2013: Turbine Technical Conference and Exposition. Volume 1A: Combustion, Fuels and Emissions. San Antonio, Texas, USA.

[9] Donini, Andrea, Bastiaans, Robert J. M., van Oijen, Jeroen A., and de Goey, L. Philip H., *The Application of Flamelet-Generated Manifold in the Modeling of Stratified Premixed Cooled Flames.* , Proceedings of the ASME Turbo Expo 2014: Turbine Technical Conference and Exposition. Volume 4B: Combustion, Fuels and Emissions. Düsseldorf, Germany.

[10] Goldin, Graham, Ren, Zhuyin, Forkel, Hendrik, Lu, Liuyan, Tangirala, Venkat, and Karim, Hasan., *Modeling CO With Flamelet-Generated Manifolds: Part 1—Flamelet Configuration.* , SAE Technical Paper 2019-01-0205, 2019

[11] Goryntsev, D., Tap, F., Tvrdojevic, M., and Priesching, P., *SI Engine Combustion and Knock Modelling Using Detailed Fuel Surrogate Models and Tabulated Chemistry* , Proceedings of the ASME Turbo Expo 2012: Turbine Technical Conference and Exposition. Volume 2: Combustion, Fuels and Emissions, Parts A and B. Copenhagen, Denmark. June 11–15, 2012. pp. 1141-1151. ASME.

[12] Hossam A. El-Asrag, Markus Braun, Assaad R. Masri, *Large eddy simulations of partially premixed ethanol dilute spray flames using the flamelet generated manifold model* , Combustion Theory and Modelling, 2020, 20:4, 567-591, DOI: 10.1080/13647830.2016.1159732

[13] Majda A., Lamb K.G. , *Simplified Equations for Low Mach Number Combustion with Strong Heat Release.* , The IMA Volumes in Mathematics and its Applications, vol 35: 167-211, 1991. Springer, New York, NY

[14] J. A. van Oijen, *Flamelet-generated manifolds : development and application to premixed laminar flames.* , Eindhoven: Technische Universiteit Eindhoven. https://doi.org/10.6100/IR557848, 2002

[15] J.A.van Oijen, A.Donini, R.J.M.Bastiaans, J.H.M.ten Thije Boonkkamp, L.P.H.de Goey *State-of-the-art in premixed combustion modeling using flamelet generated manifolds.* Progress in Energy and Combustion Science, Volume 57, November 2016, Pages 30-74

[16] L.M.Verhoeven, W.J.S.Ramaekers, J.A.van Oijen, L.P.H.de Goey *Modeling non-premixed laminar co-flow flames using flamelet-generated manifolds* Combustion and Flame, Volume 159, Issue 1, January 2012, Pages 230-241

[17] L. P. H. De Goey and J. H. M. Ten Thije Boonkkamp (1997) *A Mass-Based Definition of Flame Stretch for Flames with Finite Thickness* , Combustion Science and Technology, 122:1-6, 399-405

[18] N. Peters, *Laminar diffusion flamelet models in non-premixed turbulent combustion* , Progress in Energy and Combustion Science, Volume 10, Issue 3, 1984, Pages 319-339.

[19] N. Peters, *Local Quenching Due to Flame Stretch and Non-Premixed Turbulent Combustion* , Combustion Science and Technology , Volume 30, 1983 - Issue 1-6, Pages 1-17.

[20] Peters N. *Turbulent Combustion* , Cambridge University Publication, 2004

[21] Priesching, P., Tvrdojevic, M., Tap, F., and Meijer, C, *Prediction of the Combustion and Emission Processes in Diesel Engines Based on a Tabulated Chemistry Approach* , SAE Technical Paper 2017-01-2200, 2017, https://doi.org/10.4271/2017-01-2200.

[22] Ramaekers, W. J. S. *Development of flamelet generated manifolds for partially-premixed flame simulations.* Eindhoven: Technische Universiteit Eindhoven. https://doi.org/10.6100/IR716707

[23] S.H. Lam, D.A. Goussis, *Understanding complex chemical kinetics with computational singular perturbation* , Proc Combust Inst, 22 (1988), pp. 931-941.

[24] Tap, Ferry, Meijer, Casper, Goryntsev, Dmitry, Starikov, Anton, Tvrdojevic, Mijo, and Priesching, Peter. *Predictive CFD Modeling of Diesel Engine Combustion Using an Efficient Workflow Based on Tabulated Chemistry* , Proceedings of the ASME 2018 Internal Combustion Engine Division Fall Technical Conference. Volume 2: Emissions Control Systems; Instrumentation, Controls, and Hybrids; Numerical Simulation; Engine Design and Mechanical Development. San Diego, California, USA.

[25] U.Maas, S.B.Pope, *Simplifying chemical kinetics: Intrinsic low-dimensional manifolds in composition space* Combustion and Flame, Volume 88, Issues 3–4, March 1992, Pages 239-264